Antimicrobial Graphene Oxide Sponge for Water Treatment Applications

Anya Filina
Department of Chemical Engineering, McGill University, Montreal
November, 2018

"A Thesis submitted to McGill University in partial fulfillment of the requirements of the degree of Master in Chemical Engineering"

Abstract

Ensuring safe, reliable access to potable water remains a challenge today. Water filtration technologies based on graphene oxide sponges or hydrogels show promise in this field due to their high surface area, and versatile functionality yielding excellent adsorption affinity for different contaminants. However, the capacity for removal of bacteria and the intrinsic antimicrobial properties of graphene oxide sponges are not well understood. While composite antimicrobial systems have been successfully developed, many of these systems focus on the conjugation of antibiotics or potent metal biocides that pose cytotoxicity concerns. Natural, biologically derived antimicrobial agents such as antimicrobial enzymes, peptides and polymers hold promise in this respect due to their relatively low cost, biodegradability, biocompatibility and ability to easily functionalize graphene oxide surfaces by covalent bond formation with oxygen-containing functional groups. In the present work, the antimicrobial enzyme lysozyme, antimicrobial peptide nisin, and antimicrobial polyamide ε-poly-L-lysine were used to covalently functionalize the surface of a hierarchically porous graphene oxide sponge. The antimicrobial activity of the functionalized material was demonstrated against two model organisms: the Gram-positive *B. subtilis* and Gram-negative *E. coli.* The material performance in a simulated filtration context was evaluated using column experiments, and improved bacterial retention of both strains by the functionalized sponge was demonstrated. Furthermore, core samples of the sponge after filtration were evaluated with a membrane integrity assay and antimicrobial activity in a continuous flow mode was demonstrated.

Résumé

Assurer un accès fiable à l'eau potable reste un défi aujourd'hui. Les technologies de filtration d'eau basées sur des éponges en oxyde de graphène sont utiles dans ce contexte grâce à la structure hiérarchique des pores, la grande surface, et la bonne adsorption de divers contaminants chimiques et métalliques. Cependant, les propriétés antimicrobiennes et la capacité d'élimination des bactéries par les éponges en oxyde de graphène ne sont pas bien comprises. Bien que des systèmes composites aient été développés pour améliorer les propriétés antimicrobiennes, la plupart de ces systèmes se concentrent sur la conjugaison d'antibiotiques puissants ou de biocides de métaux qui posent des problèmes de cytotoxicité. Les agents antimicrobiens biologiquement dérivés tels que les enzymes, peptides et polymères antimicrobiens sont prometteurs, en raison de leur coût relativement peu élevé, de leur biodégradabilité, de leur biocompatibilité et de leur capacité à fonctionnaliser facilement les surfaces en oxyde de graphène par la formation de liaisons covalentes avec des groupes fonctionnels contenant de l'oxygène. Dans le présent travail, l'enzyme antimicrobienne lysozyme, le peptide antimicrobien nisin et le polyamide antimicrobien ε-poly-L-lysine ont été utilisés pour fonctionnaliser de manière covalente la surface d'une éponge d'oxyde de graphène. L'activité antimicrobienne de la nouvelle surface a été démontrée contre deux organismes modèles : *B. subtilis* en tant que Gram-positif et *E. coli* K12 en tant que Gram-négatif. La performance des matériaux dans un contexte de filtration simulé a été évaluée par des expériences sur colonne et une rétention bactérienne améliorée des deux espèces par l'éponge fonctionnalisée a été démontrée. En outre, les échantillons de l'éponge après utilisation ont été évalués et l'activité antimicrobienne en mode flux continu a été démontrée.

Acknowledgements

First and foremost, I would like to thank my supervisor Nathalie Tufenkji for providing me with the opportunity to complete this project, for her guidance throughout the process, and for her openness to my ideas and concerns. The energy and positivity that she brings to each project is remarkable. I would also like to thank her for supporting my career goals, both in industry and in academia. Her mentorship in this capacity has proven to be invaluable; and I will undoubtedly benefit from her advice in the future.

I would also like to thank the other members of the Biocolloids and Surfaces research group who have always been quick to share knowledge, and expertise. In particular I would like to thank, Nariman Yousefi, Mira Okshevsky, Heidi Jahandideh, Shawn Chahal, Nicholas Lin, Mandana Tavakolian, Arsham Hakimzadeh, Jack Minchom, Laura Hernandez, Agil Azimzada, Jeff Farner, Raphaela Allgayer. Our research group members are not only intelligent researchers but also remarkable people. Thank you for all of the coffee breaks, and philosophical/ political/ nonsensical discussions.

I would also like to thank Jean-Maxime Caron, Evgeniy Filin, Tatiana Filina, Lizzy Filine, Georges-Martin Caron, Nathalie Champagne and all of the other family and friends who reminded me of the existence of life outside of Wong building. Thank you for the time spent together, for the adventures lived, and for your love, support, and patience.

Contribution of Authors

Anya Filina performed the experimental work, data analysis, and writing tasks with the exception of those delineated below. Mira Okshevsky shared her expertise in confocal laser scanning microscopy (CLSM) and performed the CLSM image acquisition. She also provided guidance in protocol development for image analysis. Nariman Yousefi aided in XPS, FTIR and SEM measurements, and provided guidance on data analysis in the material characterization section. Nathalie Tufenkji designed the study, provided general guidance throughout the project and reviewed all written work. Chapter 2 of this thesis is a manuscript currently under review in the ACS journal *Applied Bio Materials*. All coauthors participated in reviewing and editing the manuscript.

Table of Contents

Table of Figures

Table of Tables

Chapter 1: Introduction

Water is vital to life. However, safe and reliable access to potable water is not guaranteed. Insufficient infrastructure relative to population size, industrial operations, agriculture practices, contamination events and extreme weather can all disrupt safe water access. Contaminants of concern include heavy metals, organics, pesticides, nanomaterials and pathogens [1]. Waterborne bacterial pathogens whether endemic to a region or transferred into water sources by human or animal vectors can cause potentially life threatening infectious diseases such as cholera and typhoid [2]. Recent increases in extreme weather events such as hurricanes, excessive precipitation, and seasonal monsoon or El Nino weather patterns have been documented and pose additional challenges in providing consistent, safe water supply [3, 4]. Disruption of water flow patterns can cause groundwater contamination, change pathogen concentration and increase contact with contaminated water leaving local populations vulnerable to infectious disease [3, 5, 6]. Due to the public health concerns caused by contaminated water sources, the United Nations has defined ensuring reliable, safe, drinking water access as a key goal to be achieved by 2030 [7]. However, changing weather patterns, urbanization and increased population size present new challenges and emphasize the necessity of continued research efforts in order to ensure public health and safety.

Flocculation, floatation or filtration processes are typically employed for the removal of suspended solids; while colloidal or dissolved contaminants require advanced membrane systems, chemical treatments or adsorption strategies [1]. Activated carbon based systems have been widely used both in large scale water treatment plants and small point-of-use systems due to the low energy cost and ease of operation [1]. Increasing the surface area of the adsorptive material can improve adsorption capacity, while modulating the pore structure can improve transport kinetics. Expanded or powdered activated carbon is suitable in this respect; however, the adsorptive properties of the system can be further improved by using nanoscale materials such as graphene or graphene oxide [8].

Various disinfection systems ranging from heat treatment to size exclusion technologies exist, and chlorination, ozonation and UV treatment are most frequently employed in large-scale municipal systems [1][9]. While the implementation of chemical water treatment strategies has led to documented reduction in public health risks posed by water-borne pathogens, improper selection of chemical treatment for regional water chemistry or improper dosage may cause disinfection byproducts such as trihalomethane, haloacetic acids and bromate to enter water streams, prompting many citizens to turn to the use of residential point-of-entry or point-of-use filter systems to eliminate undesirable odors and chemicals from drinking water [9].

Packed activated carbon filter systems are frequently employed in small scale point-of-use systems for the removal of chemical contaminants and even disinfection byproducts, although they are not designed for bacteria removal on their own [10]. In fact, colonization of commercial activated carbon filters by microbes has been documented in the literature [11, 12]. While these studies do not claim that a direct threat to public health exists, the decrease in water quality by microbial contamination is clearly demonstrated and biofilm formation on the filter media has the potential to dramatically decrease the efficacy of the filter media for the removal of other contaminants due to clogging or interference with adsorption sites [12, 13]. Furthermore, the lack of oversight on required frequency of filter replacement and lack of indicator systems to alert users to microbial contamination of filter media further pose challenges [11]. The development of new filtration media with the capability to both retain bacteria and prevent their proliferation by biocidal or biostatic activity has the potential to improve the efficacy and safety of water filters.

1.1 Graphene Oxide in Water Treatment Applications

1.1.1 Graphene oxide structure and synthesis

Pristine graphene consists of a single atomic layer of carbon in an sp^2 hybridized aromatic structure [14]. Through pi-pi interactions between aromatic rings, graphene sheets stack to form the lamellar structure known as graphite [14]. Synthesis of pristine graphene has been undertaken by a variety of methods, including chemical vapor deposition, mechanical exfoliation and ultrasonication [14]. Graphene oxide (GO) is the oxidized form of graphene in which the aromatic structure is disrupted in some regions and replaced by oxygen containing groups including carboxyl, hydroxyl, carbonyl, and epoxy groups [14]. These oxygen containing groups give GO a more hydrophilic character and provide sites for functionalization or contaminant adsorption. GO can be synthesized by chemical methods, most frequently the Hummers and Offeman method which uses potassium permanganate in concentrated sulfuric acid, to oxidize graphite to a GO form [15]. GO material can also be chemically reduced to the reduced graphene oxide (rGO) form which is distinct from pristine graphene due to residual functional groups and defects that form during the chemical processing [14]. The degree of oxidation correlates with color change in the material, where light material corresponds to high oxidation degree, while dark material corresponds to higher degrees of reduction [16]. Graphene based materials with a high degree of oxidation are referred to as GO, while materials with low degree of oxidation are referred to as rGO. Nevertheless, rGO materials are typically only partially reduced and may retain a large number of oxygen containing functional groups, which play an important role in the adsorption properties. For simplicity, partially reduced GO materials will be referred to as rGO throughout this work. The variability in the

degree of oxidation, hydrophilicity, sheet size, and defect density of graphene based materials contribute to their versatility and allow for their application in diverse contexts.

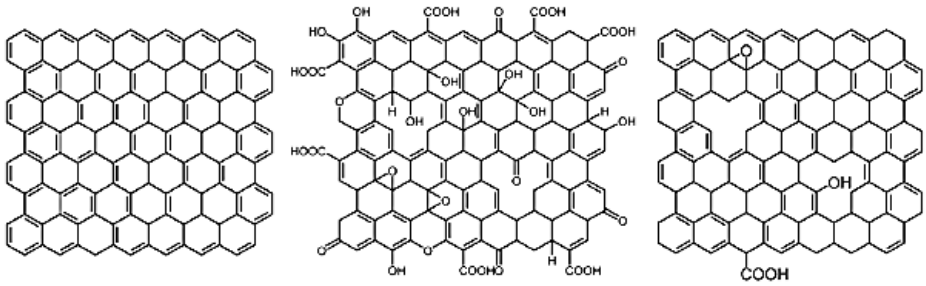

Figure 1. Schematic of graphene (left), graphene oxide (center) and reduced graphene oxide (right) [14].

1.1.2 Contaminant Adsorption

Graphene and GO based materials provide a high surface area for contaminant adsorption due to the two available basal planes. The unique chemical structure contributes to adsorption by a variety of mechanisms including electrostatic interaction, hydrogen bonding, sorption and precipitation, pi-pi interaction and hydrophobic interaction [14].

Due to the high number of oxygen containing functional groups, GO is effective at removing cationic metal contaminants such as Pb^{2+}, Hg^{2+}, Cd^{2+}, Cs^{2+}, As(III), As(V) and Cr(VI) [14]. The mechanism of metal ion adsorption is likely by electrostatic interactions between the negatively charged oxygen-containing functional groups and the metal cations [8]. An ion exchange mechanism has also been proposed where the hydronium ions adsorbed on the graphene surface become replaced by metal cations [8]. Metal contaminant adsorption is impacted by various environmental factors. Ionic strength impacts adsorption due to competition with electrolytes, and pH impacts adsorption capacity due to competition with hydronium ions at low pH and hydroxide formation at high pH [14].

Interaction of graphene based materials with organic compounds is determined by adsorbate properties such as aromaticity, dipole moment, and functional groups. Organic compounds may adsorb onto graphene oxide based systems by various interactions including hydrophobic effects, electrostatic interactions, pi-pi interactions, hydrogen bond formation and in some cases, covalent bond formation [14]. Hydrogen bonding with the hydroxylated GO surface is possible if the adsorbate has amine, hydroxyl or carboxyl functionality, while pi-pi interactions are promoted by the presence of aromatic structures in the adsorbate [14]. Electrostatic interactions occur when the adsorbate has charged functional groups. In particular, cationic dyes such as methylene blue, malachite green, rhodamine B, methyl violet,

brilliant blue efficiently adsorb to the negatively charged graphene oxide surface [8]. Adsorption of anionic dyes such as eosin Y, acid fushine, calcein, and methyl orange has also been investigated [8].

Uptake of oils and organic solvents occurs mainly through super-hydrophobic interactions, pi-pi stacking and capillarity [8]. In this respect, material systems based on reduced graphene oxide (rGO) or pristine graphene tend to be more effective than GO systems [8]. Aromatic solvents have a high affinity for graphene based systems due to pi-pi stacking interactions [8]. The characteristics of the oil such as density and viscosity all impact kinetics and adsorption capacity [8].

Due to their high affinity for a diverse array of contaminants, nanoscale graphene materials have promise in the field of water treatment. However, direct application of the nanomaterial in the water treatment context is impractical due to difficulties in removing nanoparticles from the water stream after treatment. Furthermore, the ecological and human health effects of nanoscale materials are not well understood and present cause for concern. Complexation of nanoscale GO into macrostructures allows for retention of high surface area and adsorption properties while maintaining ease of removal from the water stream post-treatment.

1.1.3 Graphene and Graphene Oxide Macrostructures

Graphene based hydrogels or sponges show promise in the water treatment field due to high surface area, continuous porous structure, high adsorption capacity and potential for recyclability. Furthermore, graphene networks promote efficient adsorption by preventing agglomeration and reduce risks of nanosheet leaching into the environment [8].

Various strategies for synthesis of graphene based macrostructures have been investigated ranging from high energy template-directed chemical vapor deposition methods to simple, self-assembly methods [8]. Direct self-assembly of GO into hydrogels depends on dispersion concentration, whereby spontaneous gelation occurs at concentrations exceeding the critical concentration [16]. The critical concentration is dictated by the degree of oxidation of the nanosheet surface. Graphene oxide is more suitable for direct self-assembly than graphene, since its hydrophilic character promotes the formation of homogenous dispersions, and the high number of functional groups allows for gelation at lower concentrations [16]. However, the mechanical strength achieved with direct self-assembly is limited [16].

Application of heat and pressure in a hydrothermal reduction process promotes network formation by pi-pi interaction, hydrogen bonding and crosslinking by epoxide and hydroxide groups [16]. Macrostructures formed by hydrothermal reduction methods have been shown to have substantially improved mechanical

properties relative to direct self-assembled materials. For instance, a robust aerogel for oil removal applications was synthesized by hydrothermal treatment and was capable of supporting 9,000 times its own weight [17].

Chemical reduction or crosslinking reactions have also been employed as a low energy alternative to produce robust graphene based networks. Acids and amines can be used as reducing agents at ambient pressures, and temperatures [16]. L-ascorbic acid, for instance, has been used as a cross-linking agent to produce high strength GO based aerogels for electronic applications [18]. Recently, L-ascorbic acid has also been employed as both soft template and reducing agent by mixing GO and cellulose nanocrystals (CNC) with an excess of L-ascorbic acid to produce a robust sponge with good adsorption properties against a variety of model contaminants [19]. This novel system produced a unique hierarchical pore structure as a result of the templating by the L-ascorbic acid which provided mass transport advantages [19]. However, it is important to note, that extremely high concentrations of reducing agent have been reported to cause shrinkage and may not be suitable for all contexts [16].

Composite systems may be employed to modulate pore structure thereby impacting adsorption kinetics. For example, morphology of the sponge may be tailored by the properties of the stabilizing agents and cross-linkers chosen. In a diamine crosslinked system, varying the length of diamines used for network formation altered the pore volume, strength, and adsorption capacity of the GO hydrogels [20]. Functionalization of GO with other materials can also improve adsorption capacity or produce systems with new functionality [14]. For instance, a GO/DNA system was able to achieve a high adsorption capacity of 960 mg/g of a cationic dye (Safarin O) due to the synergistic effect of the two negatively charged materials in the system [21]. In another system, a GO/chitosan hydrogel was capable of adsorbing both cationic and anionic dyes following incorporation of materials with both cationic and anionic character [22]. Glutathione functionalization of graphene based membranes resulted in improved removal of lead and arsenic contaminants [23]. A poly(sodium acrylate)/GO double network hydrogel was designed for the removal of heavy metal contaminants by interaction with the amino- and oxygen-containing functional groups in the composite system [24]. Composite systems have been implemented to improve the mechanical and adsorption properties of graphene oxide based systems.

Hierarchical pore structures in graphene based macrostructures provide some advantages in the context of water treatment. Adsorption kinetics in hydrogel systems are defined by three rates: the rate of contaminant diffusion through the boundary layer of the structure, rate of diffusion within the porous system and the rate of adsorption [8]. The rate of the adsorption process is frequently governed by mass

transport through the interconnected system to binding sites in the interior of the structure [8]. Macro-pores and meso-pores enable efficient mass transport kinetics, while micro-pores provide a high surface area for contaminant adsorption [8, 19]. The morphology and porosity of the structure can be adjusted by modulating the system chemistry through changes to concentration, reactant ratios, and cross-linker, and these adjustments greatly impact the pore structure, adsorption capacity and kinetics. Large pore diameters and pore volumes result in faster adsorption kinetics due to improved mass transport, while smaller hydrogel sizes and agitation of the solution can also improve mass transport [8]. While GO based networks have been studied for the removal of chemical contaminants, studies on the removal of bacteria are limited. Bacteria are an important class of contaminants that require further study.

1.2 Antimicrobial Properties of Graphene Based Materials

The intrinsic antimicrobial activity of GO and rGO has been established in the literature, yet there remains significant controversy with respect to antimicrobial potency and mechanism(s) of action [25-28]. Studies have arrived at seemingly contradictory conclusions, although upon closer inspection, the diversity of observations are likely due to variability in experimental conditions, choice of model organism, and variability in the material properties of GO itself.

1.2.1 Mechanisms of antimicrobial activity

Various mechanisms have been proposed to explain the antimicrobial properties of graphene based materials, and evidence is found in the literature to support each hypothesis.

Oxidative stress-induced membrane damage may play a key role in the antimicrobial activity of graphene based materials [25, 26]. Oxidative stress can occur due to the generation of reactive oxygen species (ROS) or by a direct electron transfer mechanism. A lipid peroxidation mechanism has been proposed in which ROS species induce a chain reaction resulting in the production of radicals which propagate the reaction causing membrane damage [29-31]. Evidence of lipid peroxidation has been observed in the presence of GO suggesting a ROS mediated mechanism [32]. However, oxidation in the absence of ROS generation has also been observed with graphene based materials of varying oxidation degrees [30], and oxidation with low ROS generation was also observed in a glutathione assay [33]. This suggests that oxidative stress by direct electron transfer may play an important role in the observed antimicrobial activity. Furthermore, in a study of GO films on various substrates, antimicrobial activity was only

observed on conducting Cu and Ge substrates, but not on the insulating silica substrate, which provides an additional line of evidence for a direct charge transfer mechanism [34].

The unique two-dimensional shape of GO may contribute to mechanical membrane damage. The nano-knife hypothesis postulates that the sharp graphene edges are capable of piercing or inserting into the cell membrane, causing destabilization of ion gradients and leakage of intracellular components [26]. A study on graphene and GO nanowalls documented the presence of intracellular components in the solution after exposure, suggesting that membrane damage and leakage of cell components occurs [28]. Computer simulations provide additional insight into the nature of membrane interactions. Simulation results suggest that lipophilic properties of graphene materials may play a key role in interactions with the cell membrane, and that pore formation rather than simple insertion may be more energetically favorable [35]. In another study, loss of cell viability was observed only upon direct contact between the bacteria and films containing immobilized GO, providing an additional line of evidence supporting mechanical damage as a key antimicrobial mechanism [31]. The nature of the membrane interactions is unclear however, since a puncture mechanism is highly dependent on the orientation, and results showed antimicrobial activity even without direct orthogonal contact with sheet edges in the fixed surface [31]. Studies on controlled alignment of GO in films provide insight into this question. In a study on the antimicrobial activity of GO against *Pseudomonas aeruginosa* and *Staphylococcus aureus*, the density of edges was a predominant factor in determining the antimicrobial activity of GO in films and evidence of disruption of membrane morphology was observed in SEM evaluations [35]. A study on the controlled orientation of GO by magnetic field alignment demonstrated increased antimicrobial potency against *E. coli* with GO in an orthogonal orientation [33]. This observation yields some support to hypotheses of membrane damage by mechanical means, although it is unclear if the edge effect is truly due to permeation of the microbial membrane by mechanical means, or whether an indirect oxidative-stress mechanism with higher defect densities at the edges plays a role.

While many studies have correlated high defect densities and small lateral size to improved antimicrobial activity, the opposite effect has been observed in nutrient rich conditions. Antimicrobial activity was shown to increase with sheet size, due to membrane wrapping mechanisms, where the nanomaterial coated the bacterial surface leading to cell entrapment and prevention of proliferation, although cell viability was not affected [31]. Higher antimicrobial efficacy with increase in lateral size of GO sheets has also been reported against *E. coli* and the mechanism appears to be the result of wrapping of the bacteria by the large GO sheets leading to nutrient depletion rather than by oxidative-stress or piercing of the cell membrane by the sharp GO edges [36]. A nutrient depletion mechanism is only relevant in

nutrient rich conditions, and therefore, the experimental environment may play a key role in the identified antimicrobial mechanism.

1.2.2 Experimental design and material property considerations

The reported antimicrobial efficacy of GO varies, and inconsistency in experimental design may contribute to the controversy. For example, there is some dispute as to whether Gram-positive or Gram-negative organisms are more susceptible to graphene based materials. Higher antimicrobial activity against Gram-negative than Gram-positive organisms has been noted in one study, and authors postulated that the thicker cell wall of Gram-positive organisms may have a protective effect against physical damage [32]. However, another study reported increased antimicrobial resistance in the Gram-negative organism *E. coli* relative to the Gram-positive *S. aureus* citing the presence of the additional outer membrane [28]. Upon closer investigation, the nutrient conditions and antimicrobial assays selected in the two studies were different and may explain the divergent trends in antimicrobial properties.

In fact, nutrient conditions may play a key role in determining the antimicrobial efficacy of GO. While antimicrobial activity of GO in low nutrient conditions has been consistently observed, the presence of nutrients, even at low concentrations, appears to decrease the antimicrobial properties of GO. One study confirmed the adsorption of nutrients onto the basal plane of GO by AFM measurements and noted a dramatic loss of antimicrobial activity against both Gram-positive and Gram-negative strains [37]. Other studies suggest that GO and r-GO may even act as a growth enhancer in nutrient-rich conditions [38-40].

Antimicrobial activity was also shown to be highly dependent on the physiological state of the bacteria. Namely, the Gram-negative *E. coli* was highly susceptible to GO when exposure took place in mid-exponential phase, while stationary phase cells showed resistance [41]. The membrane surface chemistry was demonstrated to change dramatically based on physiological phase, therefore stationary phase cells were significantly more resistant to GO [41]. Furthermore, the growth phase dependence of cell susceptibility to GO was more pronounced in Gram-negative *E. coli* as compared to Gram-positive *S. aureus* [41]. This finding highlights that the choice of organism and physiological state of the organism during exposure will significantly impact the antimicrobial effects observed. Therefore, the experimental design can significantly impact the observed trends and may partially explain the controversy surrounding the antimicrobial properties of graphene based materials.

Another key factor which likely leads to the variable antimicrobial potency observed is the variability in the properties of it material itself. Graphene oxide varies in composition, size, and degree of oxidation

and the complex interplay of material properties presents additional challenges in understanding the trends that govern antimicrobial properties. The degree of oxidation, for example, has a significant effect on the antimicrobial activity. One study found oxidized GO to have a higher antimicrobial activity than reduced rGO in a concentration- and time-dependent manner [30]. The degree of oxidation of graphene based materials is impacted by the synthesis processes, age of GO material, and environmental conditions; therefore, the antimicrobial properties of GO may be highly variable.

The effect of GO lateral size on the antimicrobial activity varies as well. In a study of the effect of graphene oxide lateral size on the Gram-negative *E. coli*, it was noted that the effect of size in suspension assays was inverse to the effect of size in film assay evaluations [31]. *E. coli* exposure in suspension showed higher antimicrobial potency in larger GO sheet size (65 μm^2), while exposure to films showed high antimicrobial activity at smaller GO sheet size (0.01 μm^2) [31]. The divergent trend suggests that the dominant antimicrobial mechanism may change depending on the context. In suspension, large GO sheets demonstrated stronger antimicrobial activity by cell entrapment mechanisms, while in films, the small sheets in surfaces showed stronger antimicrobial activity by oxidative stress mechanisms, as confirmed by glutathione assay [31]. The difficulty in testing a particular material property renders an investigation of the key mechanisms of antimicrobial activity particularly challenging. Evidence of an oxidative-stress mechanism suggests that the increased antimicrobial activity with decreasing GO sheet size was likely not the result of size itself, but was instead related to the higher defect density induced during the size-reduction ultrasonication processing [31]. The increase in defect density with decreasing lateral size is particularly relevant in redox synthesis methods such as the widely used Hummers method [25].

In the literature, the antimicrobial mechanism and effect of various material parameters is not well established. Inconsistency in experimental design, variation in cell physiology, and inability to effectively control material properties remain a challenge to understanding the antimicrobial properties of graphene based materials. However, the complexity while challenging presents opportunities for highly tunable antimicrobial material systems.

1.2.3 Graphene based materials for disinfection

Graphene oxide has been incorporated into existing filter materials in order to improve antimicrobial properties in the context of water treatment. For example, commercial cellulose nitrate membrane filters were modified with GO and poly-vinylcarbazole (PVK)/GO composite in order to impart antimicrobial properties [42]. However, the composite PVK/GO filter, rather than GO filter was more effective with up to 4 log removal achieved [42]. Presence of DNA in the filtrate demonstrated the leakage of cell

components and membrane damage [42]. Graphene based nanocomposites have also been incorporated directly as the filter medium in elution experiments for the disinfection of water [43] and jet fuel [44]. However, evidence of nanomaterial leaching into the effluent has been reported [44]. In another study, a silver nanoparticle/GO composite was developed and used to functionalize a commercial melamine sponge [45]. In an original experimental setup, strong bactericidal activity of the functionalized sponge against *E. coli* and *S. aureus* was demonstrated in a batch system where the bacterial suspension was absorbed inside the modified sponge, removed by compression, and analyzed to assess bacteria death [45]. Release of silver ions was cited to play a key role in the observed antimicrobial effects [45].

Graphene based macrostructures themselves have the potential for implementation in disinfection and water treatment systems by immobilization of bacteria and promotion of membrane damage. GO hydrogels were synthesized with agarose as the complexing agent and were capable of improved removal of *S. aureus* and *E. coli* in a gravity filtration set up compared to control agarose gels [46]. Functionalization of GO hydrogels with antimicrobial species may further improve antimicrobial properties. For instance, GO and r-GO hydrogels were developed using the cationic benzalkonium species both to promote antimicrobial activity and to act as complexing agent in self-assembly [47]. The resulting hydrogels demonstrated antimicrobial activity against both *Escherichia coli*, and *Listeria monocytogenes* [47]. As an alternative to cationic surfactant species, functionalization of graphene oxide hydrogels with bactericidal nanoparticles has also been investigated. Reduced graphene oxide hydrogels functionalized with silver nanoparticles were employed in a gravity filtration setup to disinfect water samples containing *E. coli*, yielding 35% cell inactivation where silver concentrations in the effluent were measured to be within regulatory limits [48].

While composite systems incorporating silver have proven to be effective, concerns of cytotoxicity still exist. Functionalizing graphene based hydrogels with natural, antimicrobial agents such as polymers or peptides provide a potentially safer and more sustainable alternative. The antimicrobial peptide nisin was successfully immobilized on GO by amide bond formation, and subsequently assembled into a porous hydrogel network using PEG polymer to form membranes for water treatment [49]. The small membrane pore size of 250 nm resulted in nearly complete removal of *S. aureus* from water samples [49]. Bactericidal activity at the membrane surface was determined to involve synergistic effects of membrane and oxidative stress induced by GO, which facilitated nisin binding and insertion into the membrane [49]. Functionalization of graphene based filter materials with natural antimicrobial agents has not yet been implemented in gravity filtration or column based systems.

Various classes of antimicrobial agents might be considered in the context of graphene oxide functionalization. These agents have diverse mechanisms of action and have antimicrobial effects ranging from bacteriostatic to bactericidal. However, not all antimicrobial agents are suitable in the context of water treatment. In this work, the key selection criteria for antimicrobial agents to be implemented into drinking water treatment systems were identified as low cost, extracellular mode of action, biodegradability, broad spectrum activity, safety, and potential for immobilization using functional groups found on GO.

1.3 Biologically Derived Antimicrobial Agents

1.3.1 Antimicrobial Enzymes

Antimicrobial enzymes have been used in various applications ranging from food packaging to biomedical devices [50]. Antimicrobial enzymes are typically classified based on their mode of action. The enzymes may directly reduce cell viability by disrupting cell wall and membrane components or may catalyze reactions that produce oxidative species that induce oxidative stress [50, 51]. Proteolytic enzymes catalyze the degradation of bacterial peptides, such as those found in cell structural components or adhesion proteins [50]. Polysaccharide degrading enzymes catalyze the hydrolysis of carbohydrate components such as in peptidoglycan [50]. The oxidative antimicrobial enzyme class features enzymes that catalyze external reactions that lead to the production of reactive byproducts which cause oxidative stress and reduction in cell viability [50]. However, due to the substrates required, this last enzyme class may not be suitable in simple point-of-use water treatment systems.

Antimicrobial enzymes have been immobilized on a variety of materials including metals, polymers, and nanoparticles [52-57]. Immobilization of antimicrobial enzymes may impact enzymatic activity or stability range. The effect of immobilization may be beneficial in some cases. For instance, immobilization of serine proteases on PEG functionalized GO improved the thermal stability thereby expanding the activity range [58]. However, if immobilization leads to attachment at the active site, or induces conformational changes, enzymatic activity may be lost. For example, in a horseradish peroxidase/GO system, the enzymatic activity was significantly reduced compared to the free enzyme, due to conformational changes induced by electrostatic interactions [59]. Mild, covalent immobilization methods may therefore be preferable to reduce the likelihood of conformational changes and enzyme leaching; although covalent immobilization strategies that require highly reactive species or severe chemical environments may cause enzyme deactivation as well.

Various antimicrobial enzyme candidates might be considered in the context of water treatment. Lysostaphin is a proteolytic enzyme that cleaves the penta-glycine bridge found in the peptidoglycan component of bacterial cell walls [55]. This enzyme has potent, specific, antimicrobial activity against *Staphylococcus* bacterial strains including the methicillin-resistant *Staphylococcus aureus* (MRSA) [50, 55, 60]. The narrow activity spectrum limits lysostaphin efficacy, although it might be incorporated into a modular antimicrobial system. Amylase and alkaline-pectinase are polysaccharide degrading enzymes that have been immobilized on cellulose fibers and demonstrate antimicrobial activity against Gram-positive *S. aureus*, and Gram-negative *E. coli* model organisms, showing promise for application in antimicrobial fabrics [53, 61]. Lysozyme is a polysaccharide degrading enzyme that hydrolyzes the bond between N-acetylmuramic acid and N-acetyl-D-glucosamine in the peptidoglycan structural component of bacterial cell walls [50]. Lysozyme is primarily active against Gram-positive bacterial strains although when coupled with EDTA, antimicrobial activity against Gram-negative strains has been demonstrated as well [51]. Lysozyme maintains activity at pH 6-9 and ionic strength up to 0.1 M [62]. Lysozyme has been produced on industrial scale from hen egg white and this relative ease of production leads to its low cost and application in a variety of products such as pharmaceuticals and food preservation agents [51]. Lysozyme has been immobilized on a variety of substrates including GO nanoparticles by electrostatic interaction, hydrophobic interaction, as well as by EDC/NHS chemistry [57, 63]. Lysozyme was immobilized by spontaneous physical interaction with GO and r-GO for antimicrobial membranes and demonstrated antimicrobial activity against *E. coli* [63].

1.3.2 Antimicrobial Peptides

Antimicrobial peptides are a class of ribosomal-synthesized peptides that are capable of bacteriostatic or bactericidal effects [64]. Many classes of organisms ranging from mammals to bacteria themselves produce antimicrobial peptides as a natural defense system against bacterial infection. Insects, for example, do not have an adaptive immune system and produce classes of cationic peptides called cecropins and defensins which cause bacterial cell membrane disruption and cell death [64]. Bacteriocins are produced by bacteria as a competitive strategy to inhibit growth of other bacterial strains [65]. While most bacteriocins are active against a narrow range of species, as in the case for colicins which inhibit *E. coli* strains only; other bacteriocins, such as nisin, demonstrate broad range inhibitory activity [65]. Bacteriocins derived from Gram-negative species generally have a narrower antimicrobial spectrum [65].

While some antimicrobial peptides may disrupt intracellular targets, most antimicrobial peptides target membrane components causing destabilization and damage [64]. The structural motifs and properties of

the peptides play a key role in the antimicrobial activity. For example, the cationic character of many antimicrobial peptides allows for electrostatic association with anionic lipid structures on the exterior of the bacterial cell membrane [66]. This cationic character provides antimicrobial peptides with a degree of specificity to bacterial cells, since mammalian cells typically house anionic lipid structures on the cytoplasmic side of the membrane and therefore will not associate as readily with the cationic peptide surface [66]. An alpha-helical structure is found in magainin, cecropin and many other antimicrobial peptides and their mode of action tends to be through membrane pore formation [66]. Other peptides have unusual amino acid chemistry. For instance, the tryptophan amino acid positions itself at the membrane-water interface leading to increased permeability of the membrane and formation of conductance channels [66]. Certain peptide structures have high specificity for bacteria by associating preferentially with lipopolysaccharide (LPS) [67].

Several antimicrobial peptides might be considered for water treatment systems; however, their applicability is constrained by specificity and material cost. The cationic, alpha-helical peptide, magainin has antimicrobial activity through membrane disruption and has been successfully immobilized on r-GO using EDC/NHS coupling chemistry [68]. However, the peptide is relatively expensive and is not suitable for water treatment application where low cost is a key parameter. PGLa, a cationic, alpha-helical peptide that causes destabilization of the bacterial cell membrane has also been successfully immobilized on GO and incorporated in a membrane system for water treatment applications [23]. Cecropin causes membrane disruption and pore formation [69] and has been immobilized by EDC/NHS chemistry on carboxylated polystyrene microspheres and by thiol-maleimide conjugation on poly(ethylene glycol) hydrogels [70, 71]. Melittin, a key component of honey bee venom, has lytic activity against a broad spectrum of bacteria and fungi primarily by inducing pore formation, and it has been successfully immobilized by EDC/NHS coupling on latex microspheres [70, 72-74]. Although mutant or complexed forms of melittin can exhibit potent antimicrobial activity with no cytotoxicity, wild-type melittin is hemolytic and is therefore not suitable for water treatment [74].

Nisin is a cationic bacteriocin peptide naturally produced by the *Lactococcus lactis* species in raw dairy products [75]. Nisin is most effective against Gram-positive strains such as *Listeria monocytogenes* although it is effective against Gram-negative *Escherichia coli* and *Salmonella* strains as well [76]. Furthermore, antimicrobial activity against Gram-negative strains can be improved by chelating, heating, or freezing treatments which alter cell wall structures and allow nisin to more easily contact the cytoplasmic membrane [75]. The hydrophilic c-terminal and hydrophobic n-terminal allow nisin to insert directly into the bacterial cell membrane and to form a complex with Lipid II, a precursor molecule

involved in peptidoglycan synthesis [75]. Nisin is capable of immobilizing on GO, and a recent study described the application of a nisin-functionalized GO based membrane for disinfection of *S. aureus* [49].

1.3.3 Antimicrobial Polymers

Antimicrobial polymers have been studied for food packaging, disinfecting and biomedical applications. Polymers with intrinsic antimicrobial activity eliminate dangers associated with the release of potentially cytotoxic biocidal agents [77]. Most antimicrobial polymers, whether biologically derived or synthetically produced, typically have a cationic character due to the presence of various functionalities including protonated amino groups, quaternary ammonium, quaternary phosphonium or tertiary sulfonium groups [77, 78]. The inhibitory activity of the cationic polysaccharide chitosan has been demonstrated against a range of Gram-positive and Gram-negative bacteria, and fungi, with minimum inhibitory concentrations (MIC) ranging from 0.01 mg/mL to more than 2.5 mg/mL [79]. Several antimicrobial mechanisms for chitosan have been suggested. The positively charged protonated amino group may interact with negatively charged components of the bacterial membrane causing increase in permeability and disruption of ion and concentration gradients [77]. DNA interactions and chelating action have also been proposed as possible mechanisms [77]. Chitosan and its functionalized derivatives have been applied in composite systems with GO for the development of antimicrobial networks and membranes for various applications; however, the antimicrobial efficacy of chitosan alone appears to be limited and the majority of the antimicrobial activity arises from the presence of other antimicrobial components in the system such as GO or metals [80-82]. Chitosan is not water soluble and becomes soluble only in acidic conditions, and this property restricts the range of environmental conditions that may be selected for antimicrobial assays due to stability limitations.

By contrast, the cationic polyamide ε-poly-L-lysine (PLL) is water soluble over a wide range of pH and concentrations [77]. Antimicrobial activity has been demonstrated against a broad range of Gram-positive and Gram-negative bacteria and fungal species, where the antimicrobial mechanism is related to electrostatic interaction of the cell membrane with the protonated amino groups that cause damage to the membrane, irregular cytoplasm distribution, pore formation and cell damage [83, 84]. The intrinsic antimicrobial properties of ε-poly-L-lysine have been exploited for the development of antimicrobial nanoparticles [85] and hydrogels [86]. Additionally, functionalization of GO systems with ε-poly-L-lysine for the development of antimicrobial nanocomposites has been demonstrated by direct mixing (electrostatic interactions) and covalent coupling using EDC/NHS methods [87-90]. Antimicrobial polymers have promise in the field of water treatment due to broad spectrum antimicrobial activity.

Furthermore, the antimicrobial mechanism is less specific and does not depend on the material conformation; therefore, antimicrobial polymers are less susceptible to loss of antimicrobial activity after chemical functionalization.

1.4 Objectives

The objective of this work is to develop an antimicrobial material by functionalizing the partially reduced graphene oxide sponges (sp-rGO) with natural antimicrobial agents for water treatment applications. Antimicrobial properties in a water filter context may be beneficial by allowing for more effective removal of bacteria or by preventing bacteria proliferation within the filter that may have detrimental impacts on filter efficacy and longevity. A GO sponge synthesized by chemical reduction with L-ascorbic acid was recently developed in our research group and provides certain advantages in the water treatment context due to ease of processing, hierarchical pore structure, good mechanical strength and good adsorption properties against a variety of chemical contaminants [19]. Functionalization of this material with antimicrobial agents has the potential to impart antimicrobial character to the surface thereby expanding the applicability of this material in new contexts.

While various classes of antimicrobial agents might be selected, biological amino acid based antimicrobial agents were chosen due to their biocompatibility and capacity for covalent functionalization by amide bond formation with the carboxyl groups on the GO surface. The antimicrobial enzyme lysozyme (LYS), the antimicrobial peptide nisin (NIS) and antimicrobial polyamide ε-poly-L-lysine (PLL) have all demonstrated a potential for broad spectrum antimicrobial activity, can be used to functionalize GO and are biocompatible with human cells. A systematic materials development process was undertaken in this work.

The antimicrobial activity of the selected antimicrobial agents was evaluated against two model organisms: the Gram-negative *E. coli* K12 and Gram-positive *B. subtilis* ATCC 6633 strain. While the degree of oxidation and nature of the materials are different, the possibility of functionalizing the GO sponge surface was first studied on GO nanosheet building blocks. The colloidal system allowed for better control of study conditions due to fewer mass transport limitations in suspension and the possibility of applying a greater number of standardized antimicrobial assays in a colloidal system. After demonstrating the possibility of functionalizing GO nanosheets and confirming their antimicrobial activity, a study of the GO sponge (sp-rGO) was undertaken. Functionalization of sp-rGO was undertaken by methods developed in the colloidal system. The novel functionalized material was characterized and antimicrobial activity was studied. In order to evaluate the performance of the new system, continuous

flow column transport experiments were undertaken. In the literature, elution or gravity filtration experiments with graphene based nanocomposites and sponges have measured initial and final contaminant concentrations after filtering fixed volumes of contaminated water [43, 44, 46, 48]. There are no continuous flow column transport studies on bacteria retention in graphene sponge based filtration systems. The antimicrobial activity of the spent filter material was evaluated by confocal laser scanning microscopy (CLSM) after use in a continuous flow filtration system.

Chapter 2: Antimicrobial hierarchically porous graphene oxide sponges for water treatment

Anya Filina, Nariman Yousefi, Mira Okshevsky, Nathalie Tufenkji. Manuscript in Preparation.

2.1 Introduction

Ensuring reliable access to potable water is a growing challenge today. Population growth, urbanization, and increased frequency of extreme weather events create stress on our water systems [3, 4]. Graphene oxide (GO) has shown potential as an adsorptive material for water treatment applications with a capacity to remove a variety of organic dyes, metals, and model pharmaceuticals [8, 14]. Furthermore, GO nanosheets can self-assemble into hydrogel networks or sponges that allow for removal of the filter material from the water stream after treatment [16, 18, 20-22]. Recently, our lab developed a robust and hierarchically porous, partially reduced GO sponge (sp-rGO) by reduction with L-ascorbic acid that showed promise for the removal of various classes of water contaminants [19].

While the use of GO based sponges for the removal of chemical contaminants by adsorption has been studied, the removal of bacteria by GO and rGO systems is not well understood. GO and rGO nanosheets are reported to exhibit antimicrobial properties through both oxidative stress [28, 29, 31] and membrane damage [30, 33, 36] mechanisms, although the primary antimicrobial mechanism and the extent of bactericidal potency remain unclear [25, 91]. While some proposed technologies rely on the intrinsic antimicrobial properties of GO in the context of water treatment and disinfection [42, 92], improved disinfection efficacy may be achieved in composite systems incorporating potent antimicrobial metals [45, 48], salts [93], and peptides [23, 49, 71].

Natural antimicrobial agents such as antimicrobial enzymes, peptides and polymers are promising in this context due to their biocompatibility, relatively low cost, and low toxicity. The objective of this work is to impart antimicrobial properties to the sp-rGO by functionalizing it with natural, antimicrobial agents including an enzyme (lysozyme), peptide (nisin) and polyamide (ε-poly-L-lysine). Lysozyme (LYS) catalyzes the cleavage of peptidoglycan, the primary structural component found in bacterial cell walls [50] and it has been successfully immobilized by electrostatic interactions and covalent coupling to form nanocomposites with GO [50]. The antimicrobial peptide nisin (NIS) has been coupled to GO to produce a nanocomposite based porous membrane for water disinfection [49]. The cationic polyamide ε-poly-L-lysine (PLL) has broad spectrum antimicrobial activity against both Gram-positive and Gram-negative bacteria species [77, 84]. It has been studied with GO as a nanocomposite for sensing and biomedical applications but has not yet been studied in the context of GO based 3D porous structures for water

treatment [87-90]. All three of the selected antimicrobial agents are relatively low cost, have no reported evidence of cytotoxicity to mammalian cells, and contain functional groups suitable for covalent coupling with the GO surface.

In this work, we developed antimicrobial GO nanosheets and sponges by covalently bonding LYS, NIS, and PLL to their surfaces. Antimicrobial assay with the antimicrobial agents alone were undertaken to assess their activity against the model Gram-positive *B. subtilis* 6633 and the model Gram-negative *E. coli* K12. Antimicrobial agents were immobilized on both GO nanoparticles and the sp-rGO material by EDC/NHS coupling chemistry and attachment was confirmed by X-ray Photoelectron Spectroscopy (XPS), Fourier Transform Infrared Spectroscopy (FTIR), zeta-potential measurements and Scanning Electron Microscopy (SEM). Subsequently, the antimicrobial efficacy of functionalized GO nanosheets was evaluated by assessing impact on cell growth, and cell membrane integrity. The antimicrobial activity of functionalized sp-rGO was evaluated by membrane integrity assay. While column transport experiments have been used to study bacterial transport in sand and other granular media [43, 44, 94-96] and gravity filtration experiments with graphene based networks have been conducted, [48, 93] dynamic bacterial transport in porous GO based networks has not previously been studied. To this end, performance of the functionalized sp-rGO was evaluated in continuous flow (packed column) systems by measuring bacterial removal and cell death within the sponge after use.

2.2 Materials and Methods

2.2.1 Material Synthesis

Graphene Oxide (GO) Synthesis

Graphene oxide was synthesized by a modified Hummer's synthesis method [97, 98]. Briefly, graphite (natural graphite, Ausbury Mills) was expanded at 1050℃ for 15 s. 0.5 g of expanded graphite was suspended in 100 mL of concentrated sulfuric acid (Fisher) and reacted with 5 g of potassium permanganate (Sigma Aldrich) for 24 hr with stirring at 200 rpm. Reaction temperature was maintained at 45℃ in a water bath. Following the reaction, the reaction flask was transferred to an ice bath and 125 mL of a 4:1 solution of deionized water (DI): hydrogen peroxide (Fisher) was slowly added while stirring for a total reaction time of 30 min. The mixture was then transferred to centrifuge tubes and was washed through multiple centrifugation steps. Each wash consisted of decantation of supernatant, resuspension, and centrifugation at a maximum relative centrifugal force (rcf) of 20,000*g*. A total of 3 acid wash cycles were performed in 10% hydrochloric acid (Fisher) solution, followed by 5 water wash cycles in DI water. The final GO dispersion with a concentration of 4 mg mL^{-1} is stable and may be stored at room temperature.

Graphene Oxide Sponge (sp-rGO) Synthesis

The hierarchically porous sp-rGO were prepared according to previously described methods [19]. Briefly, 6 g of vitamin C (L-ascorbic acid, Fisher) was added to 40 mg of GO in glass vials and was mixed by vortexing. The vials were subsequently held in a water bath at 95 °C for one hr. Vortexing was performed after 2, 5, and 15 min to ensure homogenous dispersion and then the vials were left undisturbed for the remainder of the hr. The self-assembled, partially reduced GO sponges were washed with large amounts of DI water to remove excess vitamin C.

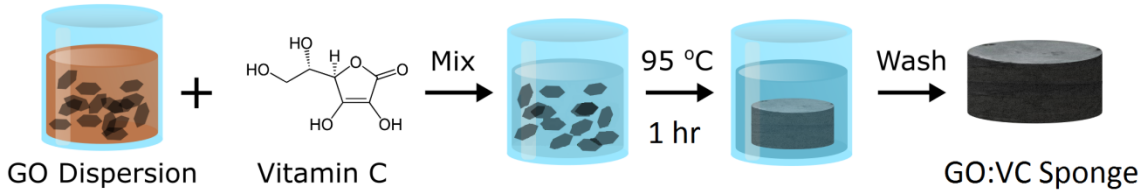

Figure 2. Schematic of sp-rGO synthesis [19].

Functionalization of GO and sp-rGO with Antimicrobial Agents

The surface of the GO nanosheets or sp-rGO material was functionalized with antimicrobial agents by amide bond formation between carboxyl groups on the GO surface and amino groups on nisin (Sigma Aldrich), lysozyme (ThermoFisher), and poly-L-lysine (Carbosynth) based on previously reported methods [23, 49]. GO surface carboxyl groups were activated by reacting with the coupling agents 1-Ethyl-3(3-dimethylaminopropyl)carbodiimide.HCl (EDC) (Sigma Aldrich) and N-hydroxysuccinimide (NHS) (Sigma Aldrich) for 30 min. Antimicrobial agents were subsequently added in varying weight ratios under stirring. Reaction was allowed to proceed for 24 hr. Excess reagents were removed by washing. Functionalized GO nanosheets were washed three times by repeating cycles of centrifugation at 20,000*g*, decantation, and re-suspension in DI. Functionalized sp-rGO was washed 10 or more times with 50mL of DI water used for each wash, and vacuum filtration was used to separate the sponge from the aqueous phase. After the final wash step, functionalized materials were stored in phosphate buffered saline (PBS, Thermo Fisher).

2.2.2 Material Characterization

Zeta Potential Measurements

Zeta-potential of functionalized nanosheets (0.04 mg/mL) in DI was measured using a ZetaSizer Nano ZS (Malvern Instruments) at 25 °C to understand impact of functionalization on surface charge. Zeta-potential correlates to surface charge and is measured at the slipping plane found between the boundary and diffuse layers surrounding a colloidal particle. Zeta-potential is measured for colloids by applying an electric field and measuring the velocity of particles in the dispersion as they move to the oppositely charged electrode. Electrophoretic mobility is determined and is used to calculate the surface charge or zeta potential.

X-ray Photoelectron Spectroscopy

The surface chemistry of the functionalized materials was studied by X-ray photoelectron spectroscopy (XPS, Thermo Scientific K-Alpha) using a monochromatic Al K_α X-ray source in 10^{-8} mbar vacuum. Thin films of GO nanosheets and free dissolved antimicrobial agents were prepared by drop casting onto aluminum foil and drying under ambient conditions. Sponge samples were freeze dried at -80 °C for 24 hr and furnace dried at 40 °C for 24 hrs. Single survey scans with pass energy of 200 eV were performed in triplicate to analyze the elemental composition and to confirm functionalization. High resolution scans with pass energy of 50 eV were performed of the C_{1s} and N_{1s} peaks. Five scans were performed for all

high resolution scans, and single scans in triplicate were performed for the survey scan measurements. XPSPEAK 4.1 software was used to de-convolute high resolution peaks into constituent peaks. Full width half maximum (FWHM) values were constrained at 0.8-1.4 eV, and Gaussian/ Lorenzian ratio was constrained between 10-30%.

Fourier-Transform Infrared Spectroscopy (FTIR) Characterization

Fourier-Transform Infrared Spectroscopy (ATR-FTIR, Perkin Elmer Spectrum Two) spectra were collected from thin-film drop cast samples of the antimicrobial agents and functionalized nanosheets and freeze-dried sponge samples. Spectra were obtained in the range of 400-4000 cm^{-1}. FTIR relies on transitions in rotational and vibrational energy states of molecules upon exposure to light in the IR range of the electromagnetic spectrum. Absorbance or transmittance values recorded over the range of excitation wavenumber values produce a spectra in which the position of peaks may be correlated to the presence of specific bonding. The spectra must be normalized to correct for baseline shift at larger wavenumbers. The normalization was performed in the equipment software package.

Scanning Electron Microscopy (SEM)

The impact of functionalization on pore structure of the sponges was evaluated by scanning electron microscopy (SEM, Hibatchi SU 2500) with secondary electrons accelerated at 5 kV. Sponge samples were cut with a razor blade to expose the interior structure and were dried by lyophilization at -80 °C for 24 hr. Samples were secured to supports using carbon tape. Sputter coating with a conductive alloy was not necessary prior to imaging, as the partially reduced GO is sufficiently conductive.

2.2.3 Evaluation of Antimicrobial Activity

Bacteria and Culture Conditions

Biosafety Level 1 model organisms were selected for antimicrobial activity assays: Gram-negative *E. coli* K12, and Gram-positive *B. subtilis* ATCC 6633. Bacteria were stored in frozen glycerol stock at -80 °C. Bacteria were streaked onto Luria broth (LB) agar (Fisher) plates and incubated overnight at 35 °C. Plates were stored at 4 °C for no more than two weeks. To prepare pre-cultures for antimicrobial assays, a single colony was selected using a sterile loop and used to inoculate 10 mL of sterile LB (Fisher) nutrient broth at a concentration of 20 g/L. For column experiments a larger volume (120 mL) of nutrient broth was required. Pre-cultures were incubated overnight at 35 °C under agitation at 130 rpm in a shaking apparatus. For experiments performed on cells in mid-exponential phase, the culture was diluted to an

OD_{600} = 0.05 and incubated again at 130 rpm at 35 °C for 4 hr for *E. coli* and 6 hr for *B. subtilis*. Prior to experiments in PBS, cells were washed 3 times, centrifuged (3,000*g*, 5 min) and resuspended in PBS.

Growth Inhibition Assay

For growth curve experiments, a pre-culture was diluted with LB nutrient broth to an OD_{600} = 0.05 and combined with the antimicrobial agent of interest in 96-well micro-titer plates. Each experiment was performed in 3 biological replicates with at least 3 technical replicates for each biological replicate. As NIS and LYS did not show evidence of inhibitory activity against *E. coli* in MIC experiments, they were not tested after immobilization on GO nanosheets.

Table 1. Summary of Experimental Conditions.

Model Bacteria	Antimicrobial Agent	Concentration range (μg/mL)	Volume ratio (bacteria : antimicrobial agent)
***B. subtilis* ATCC 6633**	**NIS**	1-32	1:1
	LYS	6-100	1:1
	PLL	16-1000	10:1*
	GO	250 -500	1:1
	GO/NIS	30:250	1:1
	GO/LYS	30:250	1:1
	GO/PLL	30-250	1:1
***Escherichia coli* K12**	**NIS**	30-250	1:1
	LYS	150-2500	1:1
	PLL	16-1000	10:1*
	GO	250- 500	1:1
	GO/PLL	30-250	1:1

*Due to the low solubility of NIS and LYS a volume ratio of 1:1 had to be used. Due to the high solubility of PLL a standard volume ratio of 10:1 (typical of MIC tests) was used which was not possible for the other materials due to solubility limitations.

Growth was tracked by optical density measurements (OD_{600}) using the Tecan Infinite M200 Pro microplate reader (Tecan Group Ltd., Switzerland). The plate was incubated at 34.5-35.5 °C. Prior to each reading, the plate was agitated in rotational mode for 1000 s. The minimum inhibitory concentration (MIC) is considered to be the lowest concentration tested with complete growth inhibition after 24 hr. The mid-exponential phase growth rate was calculated by determining the slope of the linear portion of the semi-logarithmic plot, and lag time was determined as the intersection of the linear regression of the exponential and lag portions of the semi-logarithmic growth profiles [99, 100].

Membrane Integrity Assay

Bacteria culture harvested in mid-exponential growth phase and was washed three times to remove nutrients by centrifuging 3000*g* for 5 min and re-suspending in PBS (Sigma). After the final wash, the bacteria was re-suspended in PBS to achieve a final OD_{600}=1. For Live/Dead imaging, bacteria were incubated for 15 hr with nanosheets (0.250 mg/mL) or sponge (0.125g) in PBS (200 μL total volume) in 96-well untreated microscopy plates for Live/Dead imaging (IBIDI). Subsequently, the samples were stained using the Bac-Light (Live/Dead BacLight® L13152, Molecular Probes) stain kit. The green florescent stain SYTO-9 permeates cell membranes and stains all bacteria, while the red florescent stain propidium iodide only binds to cells with compromised membranes. Samples were imaged using a Zeiss LSM800 confocal laser scanning microscope. Three biologically distinct replicates were prepared and a total of 30–50 images were obtained for each condition. Image analysis was performed using ImageJ software. Briefly, the color channels in each image were split and the pixel area of red fluorescence and total fluorescence was measured. The percentage of compromised cells was calculated as a ratio of red biomass to total biomass.

2.2.4 Removal of Bacteria by sp-rGO in Continuous Flow

A 1 cm diameter glass column (GE Life Sciences) was used for continuous flow experiments. A Nylon membrane (Spectrum Laboratories, mesh opening 70 μm) was laid onto the bottom end piece of the glass column. Next, a layer of clean acid washed [94] quartz sand (2 g, mesh size 50/70) was added. A water saturated sp-rGO sample (40 mg GO) was crushed using a metal spatula and wet-packed into the column filled with electrolyte solution. All tubing in the column apparatus were purged of air and filled with electrolyte during the column packing process. An electrolyte flowrate of 0.4 mL/min was used and the column was allowed to equilibrate until constant absorbance values were attained. A UV-vis spectrophotometer (Agilent HP8453) with a 30 μL flow cell was used to monitor the effluent bacteria concentration at a 600 nm wavelength. In addition to absorbance measurements, aliquots were collected at (t=0, 60, 120, 180 min). Effluent samples were serially diluted and plated using the drop-plate colony forming units (CFU) method [101]. 0.1X PBS buffer having an ionic strength of 0.016 M was used as the electrolyte. Confocal laser scanning microscopy (Zeiss LSM800) was used to image the bacteria present in the sponge material after use, in order to determine antimicrobial performance of the sponge material in continuous flow operation.

2.3 Results and Discussion

2.3.1 Functionalization of GO nanosheets and sponges with antimicrobial agents

The selected antimicrobial agents all contain amine groups that can be exploited for functionalization by amide bond formation with carboxyl groups on the GO nanosheet and sp-rGO surface. The antimicrobials were first immobilized on the GO nanosheets, the building blocks of the sponge, prior to functionalizing sp-rGO.

Zeta-potential Measurements

Zeta-potential (ζ) of the different nanosheets was measured to compare the surface charge of pristine GO and functionalized GO (Table 2). Zeta-potential (ζ) is a measure of electrokinetic potential of particles in colloidal systems; and while this measurement is dependent on a variety of factors including ionic strength of the solvent, under the equivalent conditions the zeta-potential may be extrapolated to infer and compare surface charge of colloidal particles.

Table 2. Summary of surface charge (zeta-potential) results for functionalized GO nanosheets for a reaction ratio of 2:1 (GO: antimicrobial agent).

Material	Zeta-Potential (ζ)
GO	-48 ± 3
GO/NIS	-27 ± 1
GO/LYS	-42 ± 1
GO/PLL	-5 ± 2

The zeta-potential of GO (0.04 mg/mL) was negative due to the high density of oxygen containing functional groups which render the surface negatively charged overall. Functionalized GO showed an increase in zeta-potential. Since all of the antimicrobial agents carry a net positive charge, and increase in surface charge is preliminary evidence of successful functionalization of the GO nanosheets. The greatest change in surface charge occurred in the GO/PLL sample which exhibits a near neutral zeta-potential.

X-ray Photoelectron Spectroscopy

XPS analysis was performed to confirm functionalization of the GO nanosheets by EDC/NHS coupling chemistry and to determine the elemental composition of the functionalized GO nanosheets. While no

nitrogen content was detected in pristine (non-functionalized) GO samples, after functionalization 6-10 at% nitrogen was detected (Table 3). Furthermore, when the ratio of NIS:GO and LYS:GO was doubled during functionalization, the at% nitrogen also approximately doubled, suggesting consistent and successful immobilization by EDC/NHS coupling chemistry (Table 3).

Table 3. Atomic composition of functionalized nanosheets.

Material	C1s	O1s	N1s
NIS	60.5 ± 2.2%	29.6 ± 0.5%	9.9 ± 1.8%
LYS	38.2 ± 8.6%	46.6 ± 11.5%	15.2 ± 3.9%
PLL	67.8 ± 0.5%	14.0 ± 0.6%	18.2 ± 0.1%
GO	53.3 ± 0.6%	46.7 ± 0.6%	n.d.*
GO/NIS (2:1)	64.9 ± 0.7 %	29.0 ± 0.3%	6.1 ± 0.1%
GO/NIS (1:1)	63.5 ± 0.6%	24.2 ± 0.9%	12.3 ± 0.6%
GO/LYS (2:1)	64.1 ± 0.2 %	30.6 ± 0.5 %	5.3 ± 0.3%
GO/LYS (1:1)	60.3 ± 0.4%	29.0 ± 0.9%	10.7±0.5%
GO/PLL (2:1)	62.7 ± 2.1%	27.3 ± 0.6%	10.1±1.6%

* n.d. signifies “none detected”

Having demonstrated successful functionalization of the GO nanosheets, functionalization of sp-rGO was undertaken. A post-synthesis process was used to avoid potential damage to the antimicrobial agents by the low pH and elevated temperature (95 °C) used during sponge synthesis. The sponge network is formed by a reduction process where vitamin C is used both as a soft template and reducing agent [19]. During the synthesis, the GO nanosheets are partially chemically reduced, which potentially decreases the number of carboxyl groups available for functionalization. Immobilization of antimicrobials on the as-synthesized sponge (sp-rGO) was confirmed by XPS; and while no nitrogen was detected in the sp-rGO controls, at ~5-6% nitrogen was detected in the functionalized sp-rGO samples (Table 4). For the same 1:1 reaction ratio immobilized on the GO nanosheets (Table 3), the atomic composition of nitrogen was ~10-11%. This suggests that the immobilization on the sponge is less effective than on the nanosheets, as expected due to the reduction of oxygen containing groups during sponge synthesis. Nonetheless, the XPS data confirms that immobilization on the sp-rGO material occurs.

Table 4. Atomic composition of functionalized sponges (sp-rGO) for a reaction ratio of 1:1.

Material	C1s	O1s	N1s
sp-rGO	84.8 ± 0.5%	15.2±0.4	n.d. *
sp-rGO/NIS	77.6 ± 2.6%	16.9 ± 1.5%	5.5 ± 1.4%
sp-rGO/LYS	77.9 ± 2.6%	16.1 ± 2.2%	6.0 ± 0.7%
sp-rGO/PLL	79.8 ± 0.65%	12.1 ± 0.4%	8.2 ± 0.2%

* n.d.: none detected

Deconvolution of the C_{1s} and N_{1s} peaks was performed to provide insight into the nature of the carbon and nitrogen bonding in the functionalized sponge materials. Representative de-convoluted spectra for sp-rGO/PLL are presented in (Figure 3). The de-convoluted peak spectra for all other conditions can be found in Appendix 3.

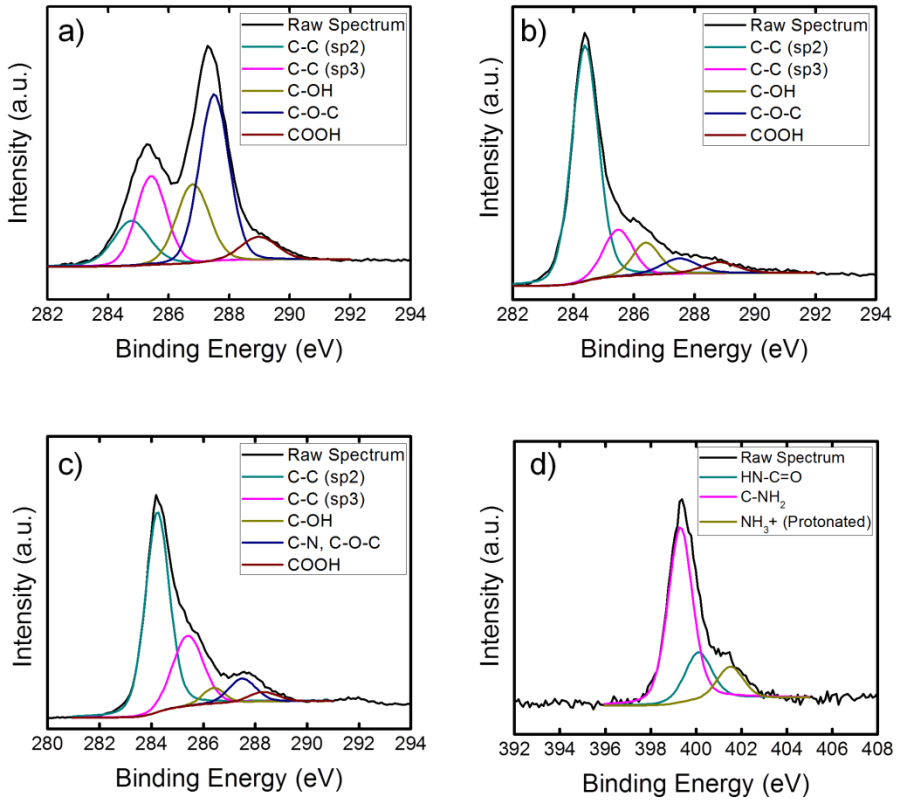

Figure 3. Deconvoluted XPS spectra of a) GO C_{1s}, b) sp-rGO C_{1s}, c) sp-rGO/PLL C_{1s}, d) sp-rGO/PLL N_{1s} peaks.

Peak positions and integrated area-based percentages are presented in Table 5. A characteristic GO C_{1s} peak profile is seen in the GO control with peaks at roughly 284.3 eV (C=C), 285.6 eV (C—C), 286.6 eV (C—OH), 287.7 eV (C=O, C—O—C), and 289 eV (O—C=O). The sp-rGO material has been partially reduced as evidenced by the large sp^2 carbon peak and lower hydroxyl, epoxide and carboxyl peaks. The change in degree of reduction of the sp-rGO was previously investigated by Raman spectroscopy, and the ratio of the D band (~1340 cm-1) to the G band (~1580 cm-1) decreased from 1.7 in GO to 1.32 in sp-rGO further confirming chemical reduction during sponge synthesis [19].

Table 5. Summary of deconvoluted C_{1s} and N_{1s} peaks in the functionalized sponge material for a reaction ratio of 1:1.

Samples	***C_{1s} Peaks***					***N_{1s} Peaks***		
	% C=C (sp^2) (~284.3 eV)	**% C–C (sp^3) (~285.6)**	**% C–OH (~286.6)**	**% C–O–C, CN (~287.7)**	**% C–OOH (~289)**	**%HN-C=O (~400 eV)**	**% C-NH_2 (~401 eV)**	**% N-N, N-O (~402)**
sp-rGO	69.7	14.2	8.6	3.7	3.7	n.d.	n.d.	n.d.
sp-rGO/NIS	67.9	17.3	6.4	5.1	3.3	68.5	17.8	13.7
sp-rGO/LYS	48.4	26.5	8.5	11.3	5.3	75.2	15.0	9.8
sp-rGO/PLL	59.9	26.1	3.7	9.5	0.8	85.3	9.8	4.8

Although the carboxyl groups on the sp-rGO are used in the functionalization process, in the sp-rGO/NIS and sp-rGO/LYS material, the percentage of carboxyl groups does not change significantly. This may be attributed to the carboxyl groups present in the NIS and LYS structures. By contrast, in the sp-rGO/PLL sample, the percentage of carboxyl groups decreases relative to the sp-rGO material. This is reasonable since PLL does not contain a large number of carboxyl groups in its structure. The largest percentage of carbon is in the sp^2 binding configuration for both the pristine and functionalized sp-rGO, suggesting that the aromatic structures of the sponge surface are still exposed and complete coverage of the sponge surface by the antimicrobial agents has not occurred. However, the sp^2 hybridized peak in all functionalized samples decreases slightly due to partial coverage of the surface by the antimicrobial agents. All functionalized samples show an increase in the 287.7 eV epoxide peak. The C—N and epoxide bonds have similar binding energy; therefore, in the functionalized sample, the increase in the 287.7 peak may be the result of carbon-nitrogen bonding in the structure.

High resolution scans of the nitrogen N1s peak also provide information about the success of immobilization. The presence of a prominent peak at 400 eV corresponds to the binding energy of the amine groups. The presence of this group suggests that the increase in nitrogen content is in fact derived from the antimicrobial agents and not from entrained nitrogen, or other contaminating species.

FTIR Characterization

ATR-FTIR spectra were obtained for the functionalized sponge samples (Figure 4) and used to corroborate the surface chemistry analysis performed by XPS. In the non-functionalized sponge samples, key peak regions were identified. A broad peak at ~3300 cm^{-1} is observed which corresponds to the OH stretching mode. This broad region may also correspond to water entrained within the sample. A large peak at 1600 cm^{-1} corresponds to C=C stretching vibrations. A slight peak at 1715 cm^{-1} is attributed to the C=O stretching vibrations in unreacted carboxyl groups. A broad peak in the range of 1300-1400 cm^{-1} can be assigned to sp^3 CH bending. In the range of 1200 cm^{-1} and 1110 cm^{-1}, peaks are assigned to C—O stretching. The peak assignments correlate well with r-GO FTIR spectra for similar materials found in the literature [87-89], however, unlike other systems, and in line with our XPS results, the sp-rGO in this study is not completely reduced as evidenced by the presence of carboxyl, hydroxyl and carbonyl peak regions. This suggests that the sponge has sufficient oxygen containing functional groups needed for functionalization with EDC/NHS coupling chemistry.

A peak corresponding with C=O stretching in the amide group NHC=O is found for NIS, LYS and PLL at 1652, 1654, and 1662 cm^{-1} respectively and this corresponds well with the amide I peak reported in the literature [49, 86, 102, 103]. This key feature found in all of the antimicrobial agents is absent in the GO and sp-rGO materials and can be used to infer successful immobilization in the functionalized samples. A second amine peak in the range of 1550 cm^{-1} corresponds to NH in plane bending, and is consistent with the amide II peak in the literature [49, 86, 102, 103]. An additive effect can be observed in the functionalized samples. In both the sp-rGO/NIS and sp-rGO/LYS samples, the spectra of the functionalized material resemble that of sp-rGO. However, after functionalization, a peak broadening occurs in the range of 1500 cm^{-1} and 1000 cm^{-1}. Individual peak positions cannot be reliably identified and the spectra of the composite materials appear to be the additive result of the constituents. By contrast, in the sp-rGO/PLL sample, while some peak broadening occurs in the range of 1000 cm^{-1}, key features of sp-rGO and PLL such as the C=O stretching peak at 1700 cm-1, C=C stretching at 1600 and the amide I peak at 1650 cm^{-1} can still be identified. The FTIR measurements corroborate the XPS data and provide additional evidence of functionalization with the selected antimicrobials.

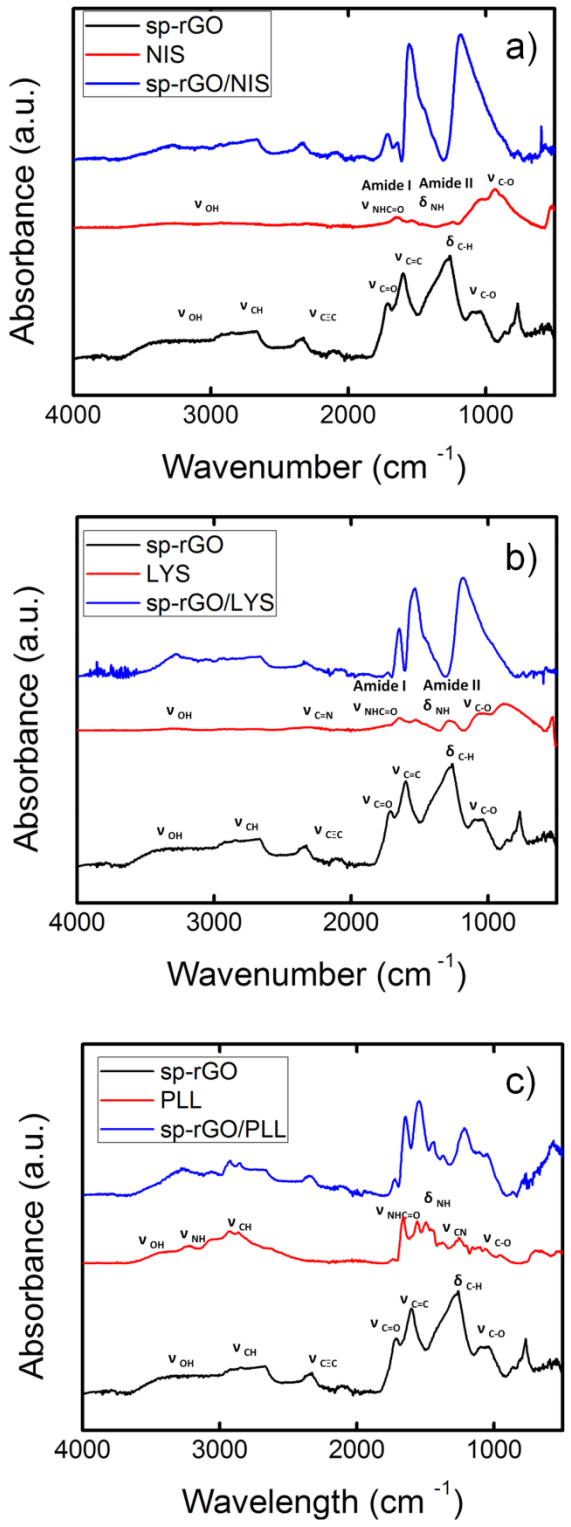

Figure 4. ATR-FT-IR spectra of pristine sponges and a) sp-rGO/NIS, b) sp-rGO/LYS, c) sp-rGO/PLL. The spectra of the antimicrobial agents alone are also shown.

2.3.2 Morphology of the sp-rGO sponges

Scanning Electron Microscopy

The pristine and functionalized sp-rGO materials were imaged by SEM to understand the effect of functionalization on pore morphology. A hierarchical porous structure consistent with our previous work on GO sponges reduced with excessive amounts of vitamin C [19] is observed in all samples. Hierarchical porosity is advantageous for the effective mass transport of contaminants while maintaining a high surface area for adsorption. In the pristine sp-rGO sample a two-tiered hierarchical structure is observed with large primary pore size on the order of 500 μm (Figure 5a). The walls of the large primary pores are composed of smaller secondary pore structures with diameters on the order of 50-100 μm (Figure 5b). SEM images show that this hierarchical pore structure is consistent in both the functionalized and pristine sponge samples (Figure 5). No apparent damage or collapse of pores is observed in the samples after functionalization suggesting that the chemical process is mild and does not damage the pore structure.

A slight expansion of the sp-rGO (Figure 5a-c) pore system is observed after functionalization with the polyamide PLL (Figure 5j-l) and both the primary and secondary pores become more open and rounded. Furthermore, the pore walls in the sp-rGO/PLL sample (Figure 5l) appear to be thinner relative to the pristine sp-rGO (Figure 5c). Exfoliation and intercalation in GO/polymer systems has been previously observed and was correlated to an expansion of the GO stacked sheet structure and increase in inter-sheet spacing [104, 105]. The pore expansion effect may provide additional benefits in the context of water treatment by improving the surface area of the sponge material and promoting large pore structures suitable for efficient mass transport. The expansion effect and thinning of the pore walls is less pronounced in the sp-rGO/NIS (Figure 5d-f) and sp-rGO/LYS (Figure 5g-i) materials, likely due to the smaller size of the NIS and LYS biomolecules as a result of the their folded structure.

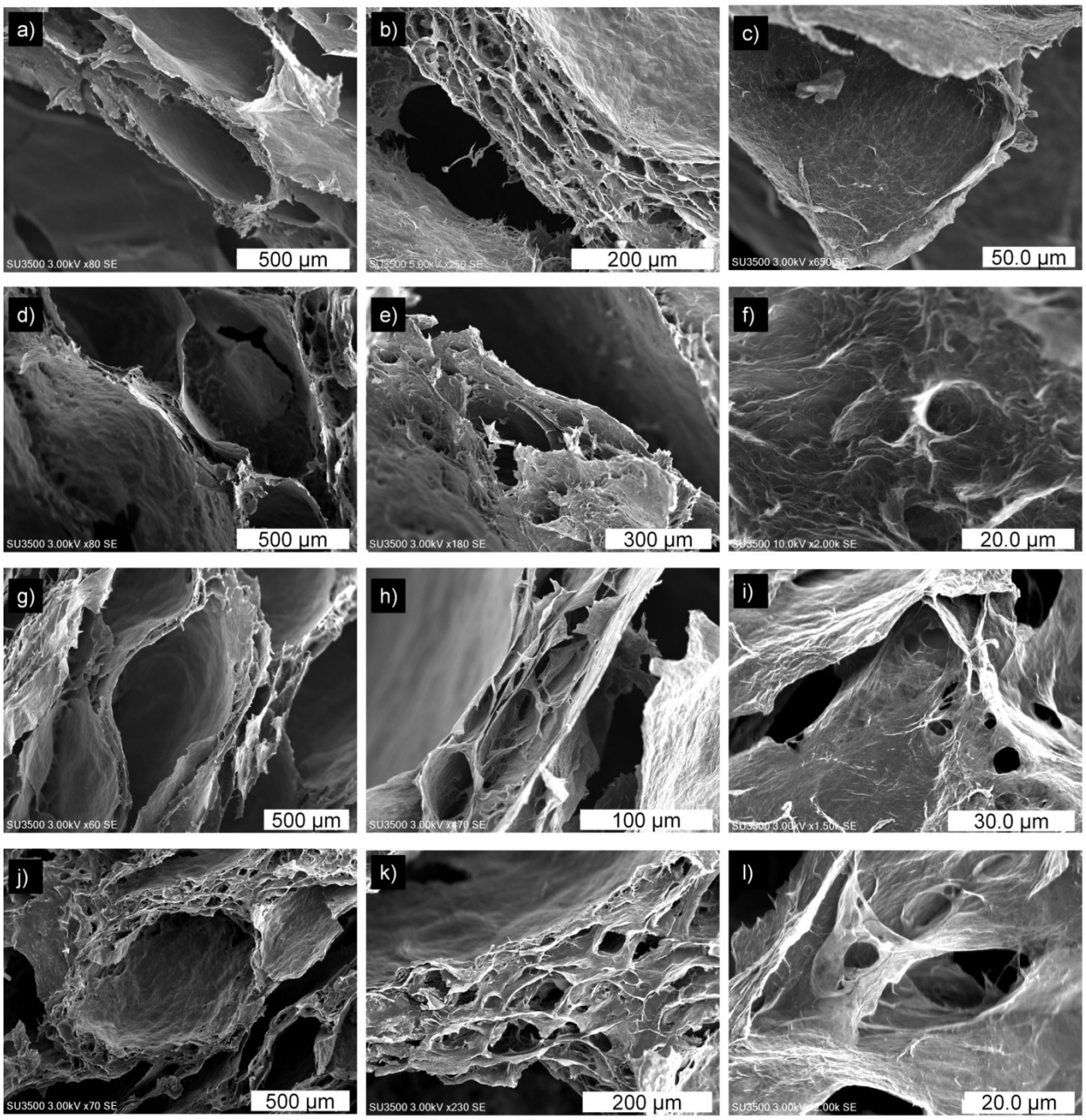

Figure 5. SEM micrographs demonstrate hierarchical porous structure in a-c) sp-rGO, d-f) sp-rGO/NIS, g-i) sp-rGO/LYS, and j-l) sp-rGO/PLL.

2.3.2 Antimicrobial Activity of Functionalized GO and sp-rGO

In-suspension growth inhibition assays

Bacterial growth curves were obtained by kinetic mode optical density measurements at various concentrations of the antimicrobial agents to estimate the minimum inhibitory concentration (MIC) of the antimicrobial agents and to observe microbial growth behavior at sub-MIC concentrations.

Table 6. Minimum inhibitory concentration (MIC) of free antimicrobial agents.

	***B. subtilis* ATCC 6633**	***E. coli* K12**
LYS	100 μg/mL	---
PLL	64 μg/mL	250 μg/mL
NIS	16 μg/mL	---

Results of MIC experiments are summarized in Table 6. All antimicrobial agents were capable of completely inhibiting growth of the model Gram-positive bacterium *B. subtilis.* However, only PLL was capable of completely inhibiting the growth of the model Gram-negative bacterium *E. coli* K12. The resistance of the Gram-negative bacterium to LYS and NIS can be explained by its outer cell membrane structure. Lysozyme causes cleavage of bonds in peptidoglycan, the structural component in bacterial cell walls [50]. In Gram-positive organisms such as *B. subtilis*, the cell wall is the outermost protective layer of the cell which allows LYS to easily access its substrate. By contrast, Gram-negative organisms such as *E. coli* have an additional outer membrane surrounding the cell wall that hinders access to peptidoglycan, and allows the cells to continue to grow even in the presence of LYS although coupling with membrane destabilizing treatments can improve antimicrobial efficacy [106, 107]. Similarly, the outer cell membrane found in Gram-negative organisms likely interferes with the mode of action of NIS [108]. While NIS completely inhibited bacterial growth in the model Gram-positive organism, complete inhibition was not observed with Gram-negative *E. coli* at the concentrations tested likely due to the presence of the outer membrane which prevents the antimicrobial peptide from accessing and inducing pore formation in the cytoplasmic membrane. At sub-MIC concentrations, extended lag phase and diminished growth rate of both *E. coli* and *B. subtilis* was observed, as described in more detail in Appendix 6.

Growth inhibition by functionalized nanosheets (GO/NIS, GO/LYS and GO/PLL)

Conservation of bacteriostatic activity of the antimicrobial agents after immobilization on the GO surface was evaluated from the bacterial growth curves (Figure 6). Measurement of antimicrobial behavior of

colloidal nanosheets poses several challenges including the color of the nanosheets themselves and potential for nanosheets aggregation during the experiment. All nanosheets were evaluated at 250 µg/mL since at this concentration the aggregation effects are minimal and do not interfere with optical density measurements as shown in Appendix 6. Although changes to bacterial growth behavior such as extended lag phase and slower growth rate were observed in the presence of functionalized GO nanosheets (Figure 6, Appendix 6), complete inhibition of growth was not achieved. It was not possibile to increase the nanosheet concentration further due to colloidal stability limitations.

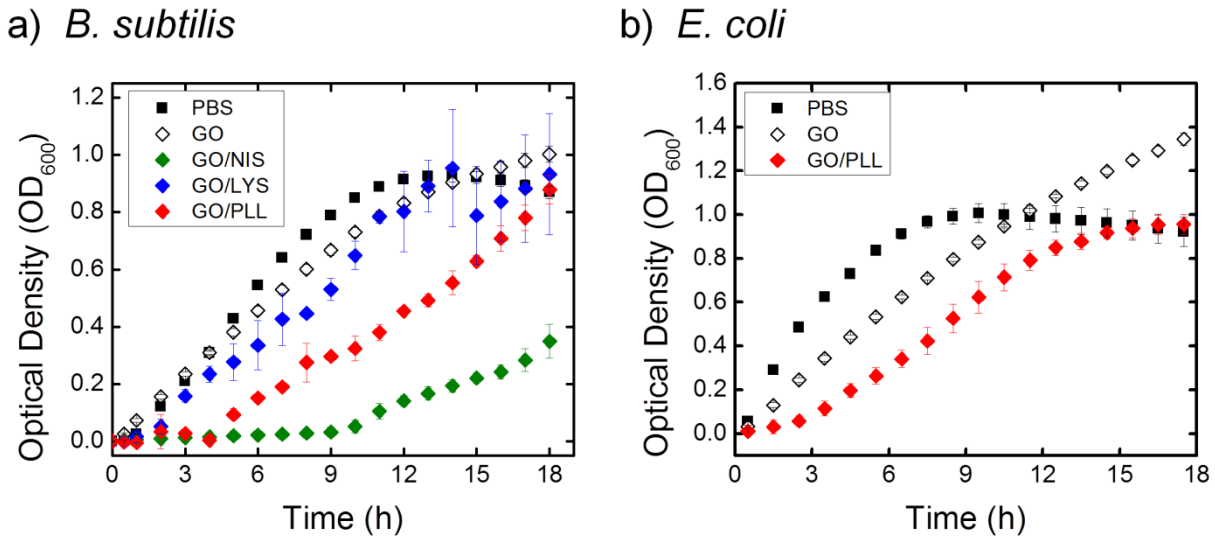

Figure 6. Representative bacterial growth curves for a) *B. subtilis* and b) *E. coli* exposed to GO and functionalized GO nanosheets. Concentration of nanosheets in all conditions was 250 µg/mL.

Semi-quantitative analysis of the lag and exponential phases of bacterial growth (Table 7) provided insight into the impact of the functionalized nanosheets on the bacterial growth dynamics. Pristine GO caused a slight decrease in growth rate but did not impact the lag phase in the organism *B. subtilis*. GO/LYS showed some antimicrobial activity against *B. subtilis* as evidenced by the slight change in growth rate. However, growth occurred at later time points to the same extent as the control condition. This may be an indication that the MIC was not reached or that antimicrobial efficacy was lost during incubation [109]. GO/NIS showed inhibitory activity against *B. subtilis* as evidenced by an extended lag phases and lower growth rate, although growth occurred at later time points. Growth of *E. coli* was only investigated with pristine GO and GO/PLL because preliminary MIC experiments with NIS and LYS did not show evidence of antimicrobial activity against this Gram-negative species (Table 6). A decrease in growth rate was observed upon exposure to the GO/PLL material.

Table 7. Key growth inhibition characteristics of *B. subtilis* and *E. coli* upon exposure to functionalized nanosheets.

	Material	Lag Phase (h)	Exponential Phase Growth Rate (Intrinsic growth rate h^{-1}, Doubling time)
***B. subtilis* ATCC 6633**	PBS Control	1 ± 0	r = 0.33 ± 0.05 Doubling time = 2.1 h
	GO	1 ± 0	r = 0.13 ± 0.04 Doubling time = 5.2 h
	GO/NIS	9 ± 1	r = 0.11 ± 0.02 Doubling time = 5.9 h
	GO/LYS	2 ± 1	r = 0.13 ± 0.02 Doubling time = 5.3 h
	GO/PLL	2 ± 1	r = 0.06 ± 0.03 Doubling time = 10.2 h
***E. coli* K12**	PBS Control	1 ± 0	r = 0.35 ± 0.07 Doubling time = 2.0 h
	GO	1 ± 0	r = 0.11 ± 0.02 Doubling time = 5.9 h
	GO/PLL	2 ± 1	r = 0.08 ± 0.02 Doubling time = 9.0 h

Loss of membrane integrity caused by functionalized nanosheets and sponges

The BacLight® membrane integrity assay provides information on biomass with damaged or compromised cell membranes. Although it cannot be assumed that all cells with compromised membranes are no longer viable, the membrane integrity assay nevertheless provides an indication of bactericidal activity of a material. Three-dimensional (z-stack) images were obtained by CLSM (Figure 7) and provide a qualitative representation of the bacterial membrane integrity after 15 hr exposure to the functionalized nanosheets. Cells with green fluorescence have an intact membrane, while cells with red fluorescence have membrane damage. The model Gram-positive organism *B. subtilis* was evaluated against GO, GO/NIS, GO/LYS and GO/PLL nanosheets. In treatments containing the functionalized GO nanosheets, increase in red fluorescence is observed relative to the pristine GO. Initial cell concentrations were equivalent, and any variance in total fluorescence can be attributed to the impermeability of GO to light. The model Gram-negative organism *E. coli* was evaluated against GO and GO/PLL nanosheets. Although there is no evidence of membrane damage in the GO/PLL condition, there is a clear aggregation effect. This is likely due to electrostatic interactions between the negatively charged bacteria and the cationic PLL. In the context of water treatment, such interactions may be advantageous, as they may lead to improved bacteria removal from the water stream.

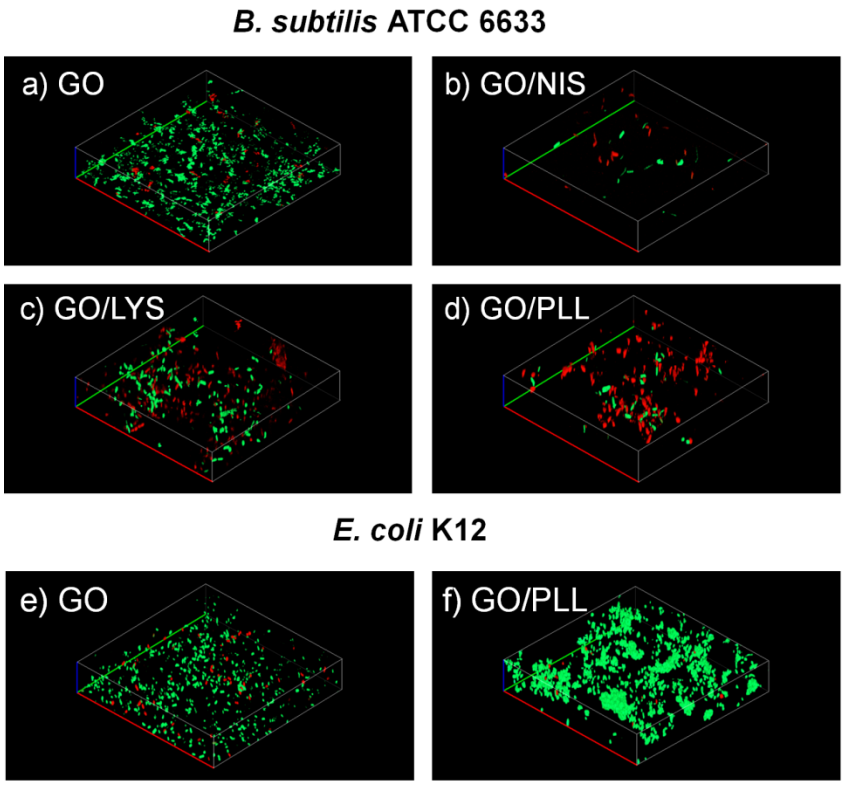

Figure 7. CLSM z-stack images of model organisms after 15 hr incubation with nanosheets in nutrient poor conditions (PBS). The conditions shown are a) *B. subtilis* with GO, b) *B. subtilis* with GO/NIS, c) *B. subtilis* with GO/LYS, d) *B. subtilis* with GO/PLL, e) *E. coli* with GO, and f) *E. coli* with GO/PLL. In all experimental conditions, nanosheet concentration was 250 µg/mL. Scale (x,y,z)= (20 µm, 100 µm, 100 µm).

For each treatment, a minimum of 30 two-dimensional images were captured and analyzed by ImageJ to quantify the relative red and green fluorescence. The Gram-positive model organism *B. subtilis* shows statistically significant membrane damage upon exposure to GO/NIS, GO/LYS and GO/PLL in nutrient poor conditions (PBS) for 15 hr (Figure 8). No statistically significant change in viability was observed following exposure to pristine GO nanosheets relative to PBS alone which suggests that increased in membrane damage with the functionalized nanosheets is attributed to the presence of the antimicrobial agents rather than to any intrinsic antimicrobial activity of GO.

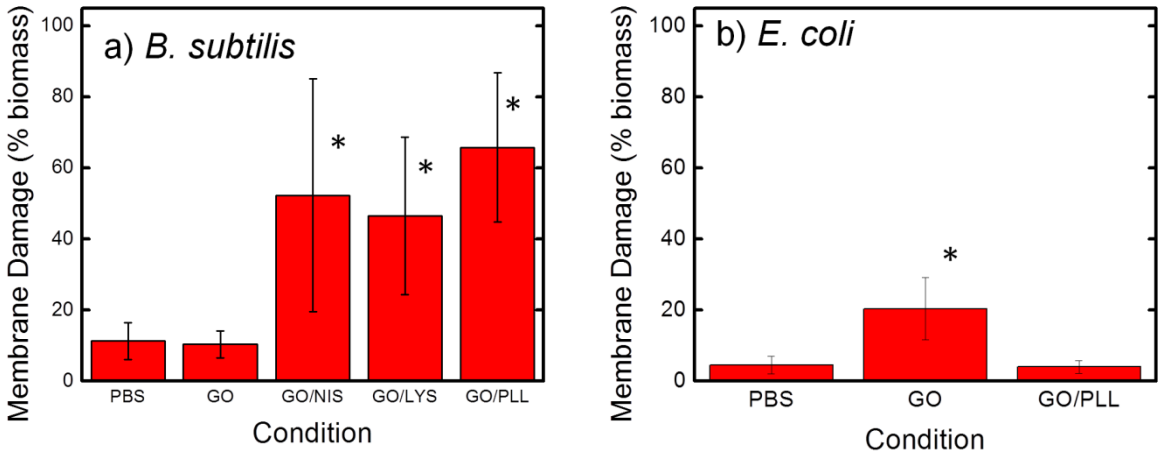

Figure 8. Membrane damage in a) *B. subtilis* 6633 and b) *E. coli* K12 exposed to functionalized nanosheets (250 µg/mL) for 15 hr in PBS. Results represent 3 biological replicates with a minimum of 30 images analyzed for each condition. Statistical significance was evaluated by the two-tailed t-test with a significance threshold of $p<0.03$.

For *E. coli,* no statistically significant membrane damage was observed with GO/PLL. However, a small but statistically significant increase in membrane damage was observed upon exposure to pristine GO. Evidence of antimicrobial activity of GO against *E. coli* and higher susceptibility of Gram-negative strains has been previously reported in the literature and is consistent with the observations in this work [41]. It has been hypothesized in the literature that the resistance of Gram-positive organisms to GO may be the result of the thicker cell wall [41]. Further investigations with greater control of material properties may lend insight into this phenomenon. The lack of antimicrobial activity in the GO/PLL condition may be attributed to concentration limitations. The MIC value of PLL against *E. coli* was substantially higher than against *B. subtilis* and this may explain the difference in membrane damage observed in these inactivation experiments. Due to limitations of the experimental method (namely, aggregation at high concentration), the concentration tested was 250 µg/mL, and the effective PLL concentration in the GO/PLL condition was less than half of the *E. coli* MIC value. Therefore, it is not surprising that significant cell death was not observed. Nonetheless, as previously highlighted, the qualitative observations of increased aggregation in the GO/PLL conditions suggest that this composite system may hold promise in the field of water treatment due to the potential for bacteria removal by physicochemical filtration.

B. subtilis ATCC 6633, E. coli K12 exposure to functionalized GO sponges

Antimicrobial activity of the functionalized sponges was confirmed with the membrane integrity assay. In suspension growth inhibition and cell inactivation assays are not well suited for evaluation of the antimicrobial activity of solid materials such as the GO sponges. Representative 3D (z-stack) CLSM images of the sponge after incubation with *B. subtilis* and *E. coli* are shown in Figure 9. The sponge material partially blocks light and therefore the images capture information about cells on the sponge surface or in sponge pore space.

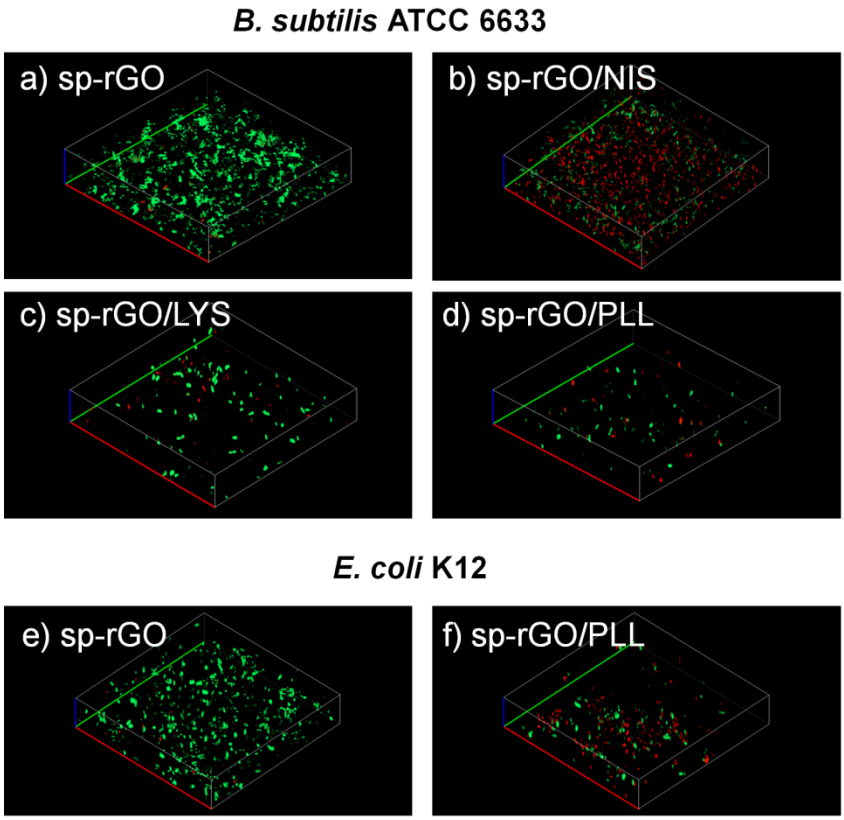

Figure 9. CLSM z-stack images of model organisms after 15 hr incubation with sponges in nutrient poor conditions (PBS). The conditions shown are a) *B. subtilis* with sp-rGO, b) *B. subtilis* with sp-rGO/NIS, c) *B. subtilis* with sp-rGO/LYS, d) *B. subtilis* with sp-rGO/PLL, e) *E. coli* with sp-rGO, and f) *E. coli* with sp-rGO/PLL. In all experimental conditions, 0.125 g of sponge and 200 µL of cell suspension (OD_{600}=1) were incubated. Images represent the sponge and buffer system. Scale (x,y,z)= (20 µm, 100 µm, 100 µm).

CLSM images were analyzed using colorimetric area based methods using ImageJ as described in the methods, and results are presented in Figure 10. The Gram-positive *B. subtilis* experienced an increase in membrane damage when exposed to the functionalized sponges relative to the pristine sp-GO and the

control (PBS alone). No statistically significant increase in membrane damage was observed in the sp-GO material relative to the PBS control. Therefore loss of cell membrane integrity upon exposure to the functionalized sponges is attributed to the presence of the antimicrobial agents rather than to antimicrobial properties of the sp-rGO itself. The antimicrobial activity of sp-rGO/Lys appears to be lower and less consistent than that of the other materials, possibly due to changes in enzyme conformation during immobilization.

The Gram-negative *E. coli* exhibited unexpected behavior in the presence of the functionalized sponges. While a statistically significant increase in cell damage was seen in the sp-rGO/PLL sample, little or no cell damage was observed in the pristine sp-rGO condition (Figure 10). This observation is noteworthy, as the GO nanosheet treatment resulted in a small but statistically significant increase in membrane damage in the same species (Figure 8). This discrepancy may be attributed in part to the difference in oxidation state of the GO material. While the GO nanosheets are highly oxidized, the sp-rGO has been partially reduced during the sponge synthesis. In the literature, a discrepancy in antimicrobial activity dependent on the oxidation state has been reported [25, 30]. Furthermore, a high density of edges has been correlated to higher antimicrobial activity of GO nanosheets [36, 110]. In sp-rGO, the partially reduced GO sheets are immobilized, thereby limiting edge effects and decreasing membrane damage by mechanical means [110]. Thus, in this study, the GO nanosheet and sp-rGO materials are not directly comparable. Future studies aimed at developing insight into the effect of oxidation state on antimicrobial activity could allow for the development of tunable GO-based antimicrobial systems.

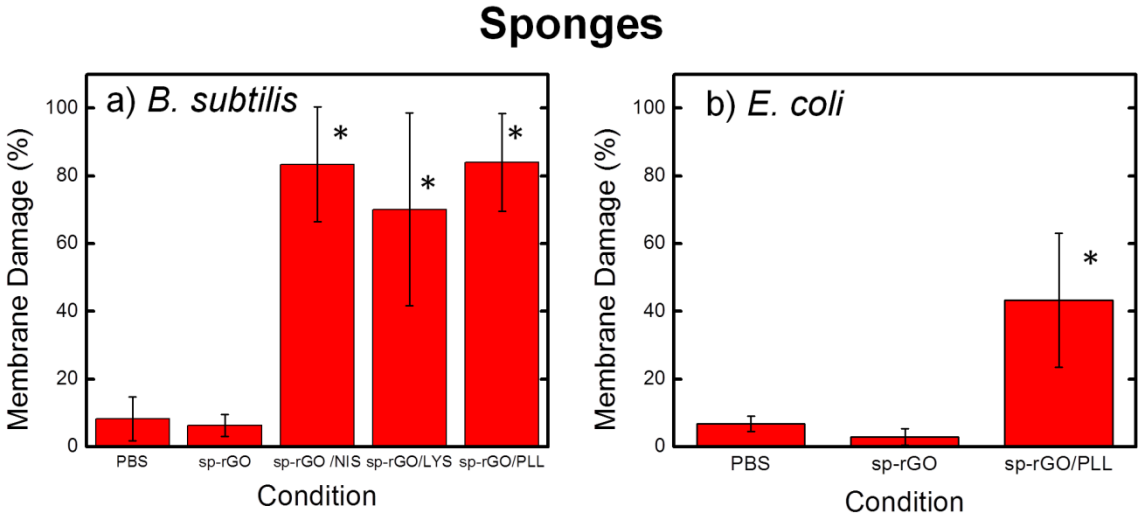

Figure 10. Membrane damage in a) *B. subtilis* 6633 and b) *E. coli* K12 exposed to functionalized sponges for 15 hr in PBS buffer. Results represent 3 biological replicates with a minimum of 30 images analyzed for each condition. Statistical significance was evaluated by the two-tailed t-test with a significance threshold of $p<0.03$.

2.3.3 Material Performance in Continuous Flow System

Removal rates of bacteria by the novel filtration medium were evaluated in a continuous flow column system. While the removal rates of various chemical contaminants using graphene based technologies have been evaluated in batch mode, [8] this configuration is less suitable to evaluate the removal of bacteria due to complex phenomena such as agglomeration, chain-forming behavior, biofilm development, and bacterial swim capability. Gravity filtration experiments have been used to study the removal of bacteria by graphene based nanocomposites [43, 44] or networks [46, 92], however, bacterial removal by graphene based macrostructures in a continuous flow mode has not been previously evaluated. A continuous flow system (packed column) set-up (Figure 11) was used to study the removal of *B. subtilis* and *E. coli* with crushed sp-rGO or sp-rGO/PLL as filter media. In these proof-of-concept experiments, only the GO/PLL material was tested as a functionalized material as it exhibited promising antimicrobial activity against both strains of bacteria (Figure 10).

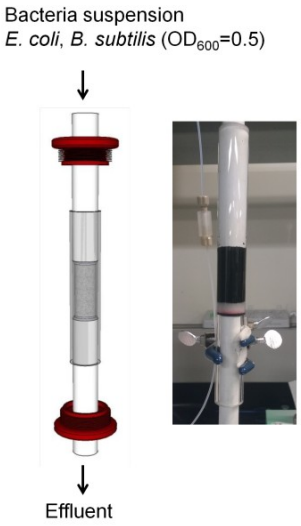

Figure 11. Schematic and photograph of packed column used in filtration experiments.

Representative bacterial breakthrough curves are shown in Figure 12. Retention of bacteria by the filter material was determined by numerical integration of the breakthrough curves to compare the performance of the functionalized sp-rGO/PLL material to the pristine sp-rGO control. The overall retention of *B. subtilis* by sp-rGO was 45%, while retention by sp-rGO/PLL was 59%. From the literature the mechanism of bacteria removal in column systems is by a combination of physicochemical attachment

and physical straining [111]. The physical properties of the sp-rGO and sp-rGO/PLL were equivalent and therefore the contribution of physical straining is likely similar in both materials. Hence, the improved bacteria retention by sp-rGO/PLL is likely the result of electrostatic interactions, due to the cationic polyamide PLL. The breakthrough profile for the sp-rGO/PLL condition shows a deflection point after 60 min revealing improved bacteria retention in the first 120 min of operation (Figure 12a). Culturability of bacteria in the effluent also decreased in the sp-rGO/PLL condition relative to the sp-rGO (Figure 12a). A slight difference in transport behavior is also observed in the flushing phase of the experiment. After 180 min of injection, the bacterial suspension was replaced with PBS. While the concentration of bacteria in the effluent began to drop immediately, in the sp-rGO column, the concentration never reached background levels suggesting that the retained bacteria was only weakly bound to the sponge and was being continuously released from the filter media. By contrast, in the sp-rGO/PLL column, the effluent concentration reached background levels more rapidly, suggesting that bacteria were more tightly bound and less likely to contaminate the filtered effluent. The kinetic measurements in this experimental set-up shed light on transport phenomena that may not be noted in batch or simple gravity filtration experiments.

Similarly, an increase in *E. coli* retention, as measured by optical density and culturability, was observed in the functionalized sp-rGO/PLL relative to the sp-rGO control (Figure 12b). The retention of *E. coli* by sp-rGO was 25%, while retention by sp-rGO/PLL was 61%. In the column packed with pristine sp-rGO, the retention of *E. coli* was lower than the retention of *B. subtilis*. The discrepancy may be related to the chain-forming behavior of *B. subtilis* (Appendix 10) which allows for physical straining to play a more significant role in bacteria retention, while in the absence of chain formation, *E. coli* may be less effectively retained by straining. Modulating the pore size and structure, packing density and flow parameters may improve filtration of a broader range of bacteria by increasing retention by both physicochemical filtration and physical straining.

The antimicrobial activity of the filter media in continuous flow mode was evaluated. Samples of the spent filter media were obtained immediately after 180 min operation, stained, and imaged by CLSM (Figure 12c-f). The percentage of *B. subtilis* cells with membrane damage was 5 ± 2% in sp-rGO and 53 ± 10% in sp-rGO/PLL. These results suggest that an antimicrobial effect is observed in a flow mode as well as in batch operation (Figure 9-10). It is important to note however, that the membrane damage was slightly higher in the batch system than in the column system. This discrepancy may be attributed to longer exposure times in the batch configuration. *E. coli* membrane damage was 2 ± 2% in sp-rGO and 31 ± 6% in sp-rGO/PLL. The increase in cell membrane damage in both model organisms upon exposure to

the functionalized sp-rGO/PLL material demonstrates that antimicrobial activity does not require extremely long contact time and antimicrobial properties are retained in a flow system.

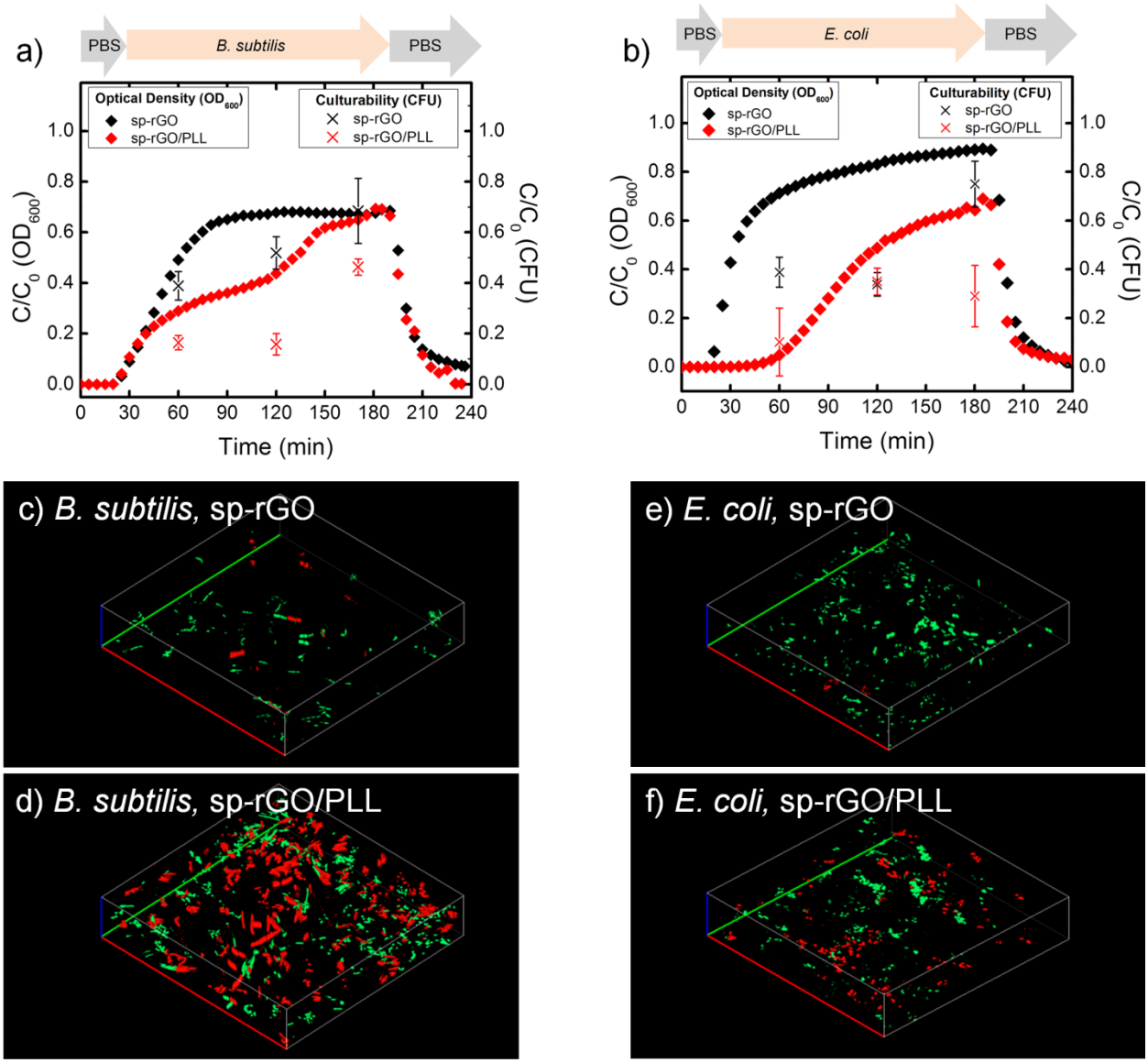

Figure 12. Representative breakthrough curves of a) *B. subtilis* 6633 and b) *E. coli* K12 (OD_{600}= 0.5) filtered through the sp-rGO and sp-rGO/PLL material. Bacteria concentration in the effluent was recorded by optical density measurements and colony counting (CFU) and is normalized to influent concentrations. Representative CLSM z-stack images of spent filter materials after 180 min use in column are also provided. Scale (x,y,z)= (20 µm, 100 µm, 100 µm).

2.4 Conclusions

Biologically-derived antimicrobial agents hold promise in antimicrobial surface applications due to their capacity for immobilization, relatively low cost, and safety. In this work, growth inhibition assays showed that while the antimicrobial agents show promise, they are not all effective against the classes of bacteria tested. Namely, NIS and LYS are only effective against the Gram-positive model organism *B. subtilis*, while PLL inhibited the growth of both *B. subtilis* and Gram-negative *E. coli*. Carbodiimide (EDC/NHS) coupling chemistry was used to successfully immobilize the selected antimicrobial agents onto first the GO nanosheet building blocks, and finally on the sp-rGO[19], previously designed for water treatment applications. Functionalization of the surface was confirmed by XPS analysis and FTIR spectroscopy. The sp-rGO material has a hierarchical pore structure, and the pores are conserved after functionalization as shown by SEM.

After functionalization, the antimicrobial activity of GO nanosheets against *B. subtilis* was improved. However, the antimicrobial activity of GO alone was more potent against *E. coli.* Antimicrobial activity of the functionalized sponge was evaluated by membrane integrity assay both in batch and continuous flow (column) systems. Increase in membrane damage upon exposure to the functionalized material was observed relative to PBS controls and pristine sp-rGO, although complete loss of viability was not achieved.

In order to gain insight into the applicability of the sp-rGO as a filtration medium, packed-column bacterial transport experiments were performed. Bacteria retention was improved in the functionalized sp-rGO/PLL material relative to the pristine sp-rGO. The improved retention of bacteria by the functionalized material is likely due to electrostatic interactions, since the physical characteristics of the filter media were equivalent. The retention of the two model bacteria varied, and it is possible that the chain forming behavior of *B. subtilis* may have contributed to additional bacterial retention by physical straining. In order to further improve bacteria retention and to develop an effective filtration system, the packing density and pore size of the sponge material could be modulated to increase the contribution of straining phenomena to bacteria retention. Characterization of spent samples of the sponge material after use in the continuous flow system showed up to ~50% membrane damage. The novel, hierarchical antimicrobial sponge exhibits improved bacteria retention in continuous flow filtration and has demonstrated improvements in antimicrobial activity in both batch and continuous flow tests.

Chapter 3: Conclusions and Future Work

While current water filter technologies have led to improvements in safe water access, many point-of use systems are not designed to remove bacteria from the water stream, and in fact colonization of filter media by microbes has been reported and can lead to lower water quality [11]. In this work, the development of an antimicrobial filter medium was undertaken by functionalized a graphene oxide based sponge with natural antimicrobial agents. The antimicrobial enzyme lysozyme, antimicrobial peptide nisin, and antimicrobial polyamide ε-poly-L-lysine where chosen for functionalization on the basis of relatively low cost, presence of amino group suitable for functionalization by amide bond formation, broad spectrum efficacy, and biocompatibility.

While the final target material was the functionalized sp-rGO, the functionalization of the GO nanosheets was studied in early stages of this work. Immobilization by electrostatic interactions was confirmed in the GO/LYS system, but was not pursued further due to the low level of immobilization and the reversible nature of the interactions. Carbodiimide chemistry (EDC/NHS) was used to functionalize the GO surface with the antimicrobial agents by covalent amide bond formation, and functionalization was confirmed by XPS and FTIR measurements. Functionalized nanosheets had an increase in at% of nitrogen relative to the pristine GO nanosheets. Furthermore, a study of the impact of reaction ratio (GO : antimicrobial agent) demonstrated that increasing the quantity of the antimicrobial agent yielded a proportional increase in at% nitrogen, suggesting that reaction is effective and is not limited by the presence of activated carboxyl groups. After determining that functionalization of the GO nanosheets by EDC/NHS coupling was possible, the post-synthesis functionalization of the sponge was undertaken and functionalization was confirmed by XPS and FTIR measurements. For comparable reaction ratios, lower nitrogen content was detected in the functionalized sp-rGO material relative to the GO material as expected due to the partial reduction of the GO surface during sponge synthesis. It is relevant to note that in the literature, EDC/NHS coupling chemistry has been used to functionalize GO nanosheets prior to complexation into hydrogel networks, [23, 49] however, in this study the possibility of a post-synthesis functionalization was demonstrated. Furthermore, SEM imaging demonstrated that the EDC/NHS chemistry used was mild enough to conserve the unique hierarchical pore structure of the sp-rGO after functionalization. Mechanical tests by rheological methods might be undertaken in the future to compare the mechanical properties of the functionalized and control sp-rGO. The results of this study demonstrate that EDC/NHS coupling chemistry is an effective method for the functionalization of both GO nanosheets and r-GO based sponges. A post-synthesis functionalization of GO hydrogels may be applied in various contexts, particularly where immobilized molecules might be damaged or altered during hydrogel synthesis.

Retention of antimicrobial activity by the antimicrobial agents after immobilization was demonstrated. Preliminary minimum inhibitory concentration (MIC) growth assay tests against the model Gram-negative organism *E. coli* K12 and the model Gram-positive organism *B. subtilis* ATCC 6633 demonstrated that while all three antimicrobial agents had antimicrobial activity against *B. subtilis,* only PLL showed antimicrobial activity against *E. coli* K12. Therefore, PLL was considered to have the most potential as a broad spectrum antimicrobial agent. Potential bacteriostatic behavior of functionalized GO nanosheets was studied and although complete inhibition of growth was not achieved, an extended lag phase and decrease in growth rate was induced by the functionalized GO nanosheets. The membrane integrity assay revealed potential bactericidal effect of the functionalized nanosheets as evidenced by statistically significant increase in membrane damage in *B. subtilis* upon exposure to functionalized GO nanosheets relative to untreated controls. No impact of GO/PLL on membrane integrity of *E. coli* K12 was observed, although some aggregation effects were noted, likely due to electrostatic interactions between the cationic PLL and anionic bacterial cell membrane.

Evaluation of the antimicrobial activity of solid and porous materials presents certain challenges since many antimicrobial assays are designed to evaluate the efficacy of molecular, soluble biocidal agents. Porous, two-phase systems have the possibility for attachment and biofouling phenomena which may confound the results of antimicrobial assays that evaluate planktonic bacteria only such as colony counting methods. For this reason, CLSM microscopy methods were used in this study to demonstrate improved antimicrobial activity of the sp-rGO after functionalization. A statistically significant increase in membrane damage was observed in *B. subtilis* upon exposure to sp-rGO/NIS, sp-rGO/LYS and sp-rGO/PLL, while no significant membrane damage was observed with the sp-rGO material. A small but statistically significant increase in membrane damage in *E. coli* was observed with the functionalized sp-rGO/PLL material relative to the control sponge and untreated conditions. These findings demonstrate that the antimicrobial properties of the sp-rGO material were improved by functionalization with the natural antimicrobial agents. Similar studies on antimicrobial peptide-functionalized GO membranes showed more than 95% bacterial inactivation by colony counting methods [23, 49] although the methodology accounted for culturability of planktonic phase bacteria removed by washing and therefore the results cannot be compared directly to the results in this work. It is relevant to note, however, that previous studies that focused on conjugation of GO hydrogels with silver nanoparticles demonstrated higher killing efficiencies of up to 99% [45, 48, 57]; while in this study, loss of viability on the order of 80% was achieved as shown by the membrane integrity assay. The superior performance of silver conjugated graphene materials is expected due to the documented broad-spectrum cytotoxicity of silver,

although leaching of silver into effluent streams has also been shown in the literature [45, 48]. Despite slightly lower killing efficiencies, the incorporation of the natural antimicrobials provides advantages in terms of biocompatibility of the filtration system.

Because of its broad spectrum antimicrobial activity and low cost, only the sp-rGO/PLL material was evaluated in filtration performance evaluations. A column apparatus was used to simulate water treatment using the porous sp-rGO material. The removal of microorganisms in filter systems occurs by physical straining and physicochemical filtration phenomena. An increase in bacteria retention by the functionalized sp-rGO/PLL material relative to the sp-rGO control was observed for both *B. subtilis* and *E. coli* strains. Since the pore and particle size was consistent between the two materials, the improved bacteria retention by sp-rGO/PLL is likely the result of electrostatic interactions. The packed column filtration system developed in this work had a removal rate of up to 61%. Similar GO or rGO sponges in the literature have reported bacterial inactivation rates ranging from 58-99% although it should be noted that removal rates of higher than 90% were only achieved in systems that incorporated silver nanoparticles [92]. Greatest bacterial removal (up to 4 log reduction) was achieved in GO hydrogel membrane systems designed to remove bacteria by size exclusion [23, 49, 92]. The pore size is a key factor in determining the efficacy of bacterial removal from the water stream; and therefore, future developments on this project should focus on modulating the pore size of the system in order to improve bacterial removal by size exclusion.

Previous studies on filter media have performed viability analysis on planktonic bacteria in the effluent stream rather than on bacteria entrained within the filter media [92]. In this study, samples of the spent filter material were imaged by CLSM microscopy to evaluate the antimicrobial properties of the material in a flow system. Membrane damage was observed in 53% of *B. subtilis* cells and 31% of *E. coli* cells in the sp-rGO/PLL material. The CLSM imaging techniques developed in this study may be applied to other systems to evaluate antimicrobial activity of filter media in continuous flow systems.

These results suggest that the functionalized sp-rGO/PLL material shows promise as a filter material, both to remove bacteria from the water stream and to reduce viability of bacteria trapped within the filter medium. The system might be improved further by modulating the pore size of the sponge material, altering column packing and flow parameters, and increasing the quantity of the antimicrobial agent in the system. Anti-biofouling potential of the functionalized sponge against biofilm forming species might be evaluated during long-term use in a continuous flow water treatment system. Other natural antimicrobial agents might also be investigated.

References

1. Burton, F.L. and D. Stensel, *Wastewater Engineering: Treatment and Reuse*. 4 ed. Vol. . 2003, New York: McGraw-Hill Companies Inc.
2. Cabral, J.P.S., *Water microbiology. Bacterial pathogens and water.* International Journal of Environmental Research and Public Health, 2010. **7**(10): p. 3657-3703.
3. Andrade, L., et al., *Surface water flooding, groundwater contamination, and enteric disease in developed countries: A scoping review of connections and consequences.* Environmental Pollution, 2018. **236**: p. 540-549.
4. Cann, K.F., et al., *Extreme water-related weather events and waterborne disease.* Epidemiology and Infection, 2013. **141**(4): p. 671-686.
5. Taylor, J., et al., *Flood management: Prediction of microbial contamination in large-scale floods in urban environments.* Environment International, 2011. **37**(5): p. 1019-1029.
6. Watkins, R.R., *Gastrointestinal infections in the setting of natural disasters.* Current Infectious Disease Reports, 2012. **14**(1): p. 47-52.
7. *Sustainable Development Goals: Clean Water and Sanitation*. 2016 [cited 2016 October 15]; Available from: http://www.un.org/sustainabledevelopment/water-and-sanitation/.
8. Shen, Y., Q. Fang, and B. Chen, *Environmental applications of three-dimensional graphene-based macrostructures: Adsorption, transformation, and detection.* Environmental Science and Technology, 2015. **49**(1): p. 67-84.
9. Enforcement, D.o.E., *Water Treatment Manual: Disinfection*, E.P. Agency, Editor. 2011.
10. Stalter, D., et al., *Point-of-use water filters can effectively remove disinfection by-products and toxicity from chlorinated and chloraminated tap water.* Environmental Science: Water Research and Technology, 2016. **2**(5): p. 875-883.
11. Nriagu, J., et al., *Influence of household water filters on bacteria growth and trace metals in tap water of Doha, Qatar.* Scientific Reports, 2018. **8**(1).
12. Vignola, M., et al., *Medium shapes the microbial community of water filters with implications for effluent quality.* Water Research, 2018. **129**: p. 499-508.
13. Daschner, F.D., et al., *Microbiological contamination of drinking water in a commercial household water filter system.* European Journal of Clinical Microbiology and Infectious Diseases, 1996. **15**(3): p. 233-237.
14. Perreault, F., A. Fonseca De Faria, and M. Elimelech, *Environmental applications of graphene-based nanomaterials.* Chemical Society Reviews, 2015. **44**(16): p. 5861-5896.
15. Hummers, W.S. and R.E. Offeman, *Preparation of Graphitic Oxide.* Journal of the American Chemical Society, 1958. **80**(6): p. 1339.
16. Fang, Q., Y. Shen, and B. Chen, *Synthesis, decoration and properties of three-dimensional graphene-based macrostructures: A review.* Chemical Engineering Journal, 2015. **264**: p. 753-771.
17. Wu, Z.Y., et al., *Carbon nanofiber aerogels for emergent cleanup of oil spillage and chemical leakage under harsh conditions.* Scientific Reports, 2014. **3**.
18. Zhang, X., et al., *Mechanically strong and highly conductive graphene aerogel and its use as electrodes for electrochemical power sources.* Journal of Materials Chemistry, 2011. **21**(18): p. 6494-6497.
19. Yousefi, N., et al., *Hierarchically porous, ultra-strong reduced graphene oxide-cellulose nanocrystal sponges for exceptional adsorption of water contaminants.* Nanoscale, 2018. **10**(15): p. 7171-7184.

20. Luan, V.H., et al., *The molecular level control of three-dimensional graphene oxide hydrogel structure by using various diamines.* Chemical Engineering Journal, 2014. **246**: p. 64-70.
21. Xu, Y., et al., *Three-dimensional self-assembly of graphene oxide and DNA into multifunctional hydrogels.* ACS Nano, 2010. **4**(12): p. 7358-7362.
22. Chen, Y., et al., *Graphene oxide-chitosan composite hydrogels as broad-spectrum adsorbents for water purification.* Journal of Materials Chemistry A, 2013. **1**(6): p. 1992-2001.
23. Viraka Nellore, B.P., et al., *Bio-Conjugated CNT-Bridged 3D Porous Graphene Oxide Membrane for Highly Efficient Disinfection of Pathogenic Bacteria and Removal of Toxic Metals from Water.* ACS Applied Materials and Interfaces, 2015. **7**(34): p. 19210-19218.
24. Xu, R., et al., *New double network hydrogel adsorbent: Highly efficient removal of Cd(II) and Mn(II) ions in aqueous solution.* Chemical Engineering Journal, 2015. **275**: p. 179-188.
25. Szunerits, S. and R. Boukherroub, *Antibacterial activity of graphene-based materials.* Journal of Materials Chemistry B, 2016. **4**(43): p. 6892-6912.
26. Zou, X., et al., *Mechanisms of the Antimicrobial Activities of Graphene Materials.* Journal of the American Chemical Society, 2016. **138**(7): p. 2064-2077.
27. Wu, X., et al., *Graphene oxide as an efficient antimicrobial nanomaterial for eradicating multi-drug resistant bacteria in vitro and in vivo.* Colloids and Surfaces B: Biointerfaces, 2017. **157**: p. 1-9.
28. Akhavan, O. and E. Ghaderi, *Toxicity of graphene and graphene oxide nanowalls against bacteria.* ACS Nano, 2010. **4**(10): p. 5731-5736.
29. Gurunathan, S., et al., *Oxidative stress-mediated antibacterial activity of graphene oxide and reduced graphene oxide in Pseudomonas aeruginosa.* International Journal of Nanomedicine, 2012. **7**: p. 5901-5914.
30. Liu, S., et al., *Antibacterial activity of graphite, graphite oxide, graphene oxide, and reduced graphene oxide: Membrane and oxidative stress.* ACS Nano, 2011. **5**(9): p. 6971-6980.
31. Perreault, F., et al., *Antimicrobial Properties of Graphene Oxide Nanosheets: Why Size Matters.* ACS Nano, 2015. **9**(7): p. 7226-7236.
32. Krishnamoorthy, K., et al., *Antibacterial efficiency of graphene nanosheets against pathogenic bacteria via lipid peroxidation.* Journal of Physical Chemistry C, 2012. **116**(32): p. 17280-17287.
33. Lu, X., et al., *Enhanced antibacterial activity through the controlled alignment of graphene oxide nanosheets.* Proceedings of the National Academy of Sciences of the United States of America, 2017. **114**(46): p. E9793-E9801.
34. Li, J., et al., *Antibacterial activity of large-area monolayer graphene film manipulated by charge transfer.* Scientific Reports, 2014. **4**.
35. Pham, V.T.H., et al., *Graphene Induces Formation of Pores That Kill Spherical and Rod-Shaped Bacteria.* ACS Nano, 2015. **9**(8): p. 8458-8467.
36. Liu, S., et al., *Lateral dimension-dependent antibacterial activity of graphene oxide sheets.* Langmuir, 2012. **28**(33): p. 12364-12372.
37. Hui, L., et al., *Availability of the basal planes of graphene oxide determines whether it is antibacterial.* ACS Applied Materials and Interfaces, 2014. **6**(15): p. 13183-13190.
38. Wu, P.C., et al., *Graphene oxide conjugated with polymers: A study of culture condition to determine whether a bacterial growth stimulant or an antimicrobial agent?* Journal of Nanobiotechnology, 2018. **16**(1).
39. Ruiz, O.N., et al., *Graphene oxide: a nonspecific enhancer of cellular growth.* ACS Nano, 2011. **5**(10): p. 8100-8107.

40. Wang, D., et al., *Using graphene oxide to enhance the activity of anammox bacteria for nitrogen removal.* Bioresource Technology, 2013. **131**: p. 527-530.
41. Karahan, H.E., et al., *Bacterial physiology is a key modulator of the antibacterial activity of graphene oxide.* Nanoscale, 2016. **8**(39): p. 17181-17189.
42. Musico, Y.L.F., et al., *Surface modification of membrane filters using graphene and graphene oxide-based nanomaterials for bacterial inactivation and removal.* ACS Sustainable Chemistry and Engineering, 2014. **2**(7): p. 1559-1565.
43. Hussein, M.A., et al., *Efficient water disinfection using hybrid polyaniline/graphene/carbon nanotube nanocomposites.* Environmental Technology (United Kingdom), 2018: p. 1-12.
44. Ruiz, O.N., et al., *Graphene oxide-based nanofilters efficiently remove bacteria from fuel.* International Biodeterioration and Biodegradation, 2015. **97**: p. 168-178.
45. Deng, C.H., et al., *Preparation of melamine sponge decorated with silver nanoparticles-modified graphene for water disinfection.* Journal of Colloid and Interface Science, 2017. **488**: p. 26-38.
46. Wang, Y., et al., *A facile and green method to fabricate graphene-based multifunctional hydrogels for miniature-scale water purification.* RSC Advances, 2013. **3**(24): p. 9240-9246.
47. Wang, X., et al., *A facile one-pot method to two kinds of graphene oxide-based hydrogels with broad-spectrum antimicrobial properties.* Chemical Engineering Journal, 2014. **260**: p. 331-337.
48. Zeng, X., et al., *Silver/Reduced Graphene Oxide Hydrogel as Novel Bactericidal Filter for Point-of-Use Water Disinfection.* Advanced Functional Materials, 2015. **25**(27): p. 4344-4351.
49. Kanchanapally, R., et al., *Antimicrobial peptide-conjugated graphene oxide membrane for efficient removal and effective killing of multiple drug resistant bacteria.* RSC Advances, 2015. **5**(24): p. 18881-18887.
50. Thallinger, B., et al., *Antimicrobial enzymes: An emerging strategy to fight microbes and microbial biofilms.* Biotechnology Journal, 2013. **8**(1): p. 97-109.
51. Fuglsang, C.C., et al., *Antimicrobial enzymes: Applications and future potential in the food industry.* Trends in Food Science and Technology, 1995. **6**(12): p. 390-396.
52. Conte, A., M. Sinigaglia, and M.A. Del Nobile, *Antimicrobial effectiveness of lysozyme immobilized on polyvinylalcohol- based film against Alicyclobacillus acidoterrestris.* Journal of Food Protection, 2006. **69**(4): p. 861-865.
53. Ibrahim, N.A., et al., *Antimicrobial activity of cotton fabrics containing immobilized enzymes.* Journal of Applied Polymer Science, 2007. **104**(3): p. 1754-1761.
54. Lian, Z.X., et al., *Preparation and characterization of immobilized lysozyme and evaluation of its application in edible coatings.* Process Biochemistry, 2012. **47**(2): p. 201-208.
55. Miao, J., et al., *Lysostaphin-functionalized cellulose fibers with antistaphylococcal activity for wound healing applications.* Biomaterials, 2011. **32**(36): p. 9557-9567.
56. Zhang, Y., et al., *Assembly of graphene oxide-enzyme conjugates through hydrophobic interaction.* Small, 2012. **8**(1): p. 154-159.
57. Eby, D.M., H.R. Luckarift, and G.R. Johnson, *Hybrid antimicrobial enzyme and silver nanoparticle coatings for medical Instruments.* ACS Applied Materials and Interfaces, 2009. **1**(7): p. 1553-1560.
58. Jin, L., et al., *Functionalized graphene oxide in enzyme engineering: A selective modulator for enzyme activity and thermostability.* ACS Nano, 2012. **6**(6): p. 4864-4875.
59. Zhang, J., et al., *Graphene oxide as a matrix for enzyme immobilization.* Langmuir, 2010. **26**(9): p. 6083-6085.
60. Yeroslavsky, G., et al., *Antibacterial and antibiofilm surfaces through polydopamine-assisted immobilization of lysostaphin as an antibacterial enzyme.* Langmuir, 2015. **31**(3): p. 1064-1073.

61. Kashyap, D.R., et al., *Applications of pectinases in the commercial sector: A review.* Bioresource Technology, 2001. **77**(3): p. 215-227.
62. Davies, R.C., A. Neuberger, and B.M. Wilson, *The dependence of lysozyme activity on pH and ionic strength.* BBA - Enzymology, 1969. **178**(2): p. 294-305.
63. Duan, L., et al., *Graphene immobilized enzyme/polyethersulfone mixed matrix membrane: Enhanced antibacterial, permeable and mechanical properties.* Applied Surface Science, 2015. **355**: p. 436-445.
64. Li, Y., et al., *Overview on the recent study of antimicrobial peptides: Origins, functions, relative mechanisms and application.* Peptides, 2012. **37**(2): p. 207-215.
65. Snyder, A.B. and R.W. Worobo, *Chemical and genetic characterization of bacteriocins: Antimicrobial peptides for food safety.* Journal of the Science of Food and Agriculture, 2014. **94**(1): p. 28-44.
66. Epand, R.M. and H.J. Vogel, *Diversity of antimicrobial peptides and their mechanisms of action.* Biochimica et Biophysica Acta - Biomembranes, 1999. **1462**(1-2): p. 11-28.
67. Koon Lim, S., et al., *Peptide-assembled graphene oxide as fluorescent turn-on sensor for ultrasensitive Lipopolysaccharide (Endotoxin) detection.* Asian Pacific Journal of Tropical Disease, 2014. **4**(3): p. 223.
68. Chen, Y., et al., *Electronic detection of bacteria using holey reduced graphene oxide.* ACS Applied Materials and Interfaces, 2014. **6**(6): p. 3805-3810.
69. Strauss, J., et al., *Binding, inactivation, and adhesion forces between antimicrobial peptide cecropin P1 and pathogenic E. coli.* Colloids and Surfaces B: Biointerfaces, 2010. **75**(1): p. 156-164.
70. Taitt, C.R., et al., *Surface Modification and Biomolecule Immobilization on Polymer Spheres for Biosensing Applications*, in *Biomedical Nanotechnology: Methods and Protocols*, S.J. Hurst, Editor. 2011, Humana Press: Totowa, NJ. p. 77-94.
71. Cole, M.A., T.F. Scott, and C.M. Mello, *Bactericidal Hydrogels via Surface Functionalization with Cecropin A.* ACS Biomaterials Science and Engineering, 2016. **2**(11): p. 1894-1904.
72. Sani, M.A. and F. Separovic, *How Membrane-Active Peptides Get into Lipid Membranes.* Accounts of Chemical Research, 2016. **49**(6): p. 1130-1138.
73. Wu, X. and G. Narsimhan, *Synergistic effect of low power ultrasonication on antimicrobial activity of melittin against Listeria monocytogenes.* LWT - Food Science and Technology, 2017. **75**: p. 578-581.
74. Wu, X., et al., *Characterization of antimicrobial activity against Listeria and cytotoxicity of native melittin and its mutant variants.* Colloids and Surfaces B: Biointerfaces, 2016. **143**: p. 194-205.
75. Adem Gharsallaoui, N.O., Catherine Joly & Pascal Degraeve, *Nisin as a Food Preservative: Part 1: Physicochemical Properties, Antimicrobial Activity, and Main Uses.* Critical Reviews in Food Science and Nutrition, 2015. **56**(8): p. 1262-1274.
76. Gálvez, A., et al., *Bacteriocin-based strategies for food biopreservation.* International Journal of Food Microbiology, 2007. **120**(1-2): p. 51-70.
77. Santos, M.R.E., et al., *Recent developments in antimicrobial polymers: A review.* Materials, 2016. **9**(7).
78. Ng, V.W.L., et al., *Antimicrobial hydrogels: A new weapon in the arsenal against multidrug-resistant infections.* Advanced Drug Delivery Reviews, 2014. **78**: p. 46-62.
79. Goy, R.C., D. De Britto, and O.B.G. Assis, *A review of the antimicrobial activity of chitosan.* Polimeros, 2009. **19**(3): p. 241-247.

80. Grande, C.D., et al., *Chitosan Cross-Linked Graphene Oxide Nanocomposite Films with Antimicrobial Activity for Application in Food Industry.* Macromolecular Symposia, 2017. **374**(1).
81. Huang, J.F., et al., *A Hydrogel-Based Hybrid Theranostic Contact Lens for Fungal Keratitis.* ACS Nano, 2016. **10**(7): p. 6464-6473.
82. Jones, S., et al., *Multifunctional Three-Dimensional Chitosan/Gold Nanoparticle/Graphene Oxide Architecture for Separation, Label-Free SERS Identification of Pharmaceutical Contaminants, and Effective Killing of Superbugs.* ACS Sustainable Chemistry and Engineering, 2017. **5**(8): p. 7175-7187.
83. Najjar, M.B., D. Kashtanov, and M.L. Chikindas, *ε-Poly-l-lysine and nisin A act synergistically against Gram-positive food-borne pathogens Bacillus cereus and Listeria monocytogenes.* Letters in Applied Microbiology, 2007. **45**(1): p. 13-18.
84. Shima, S., et al., *Antimicrobial action of<inf>E</inf>-poly-<inf>L</inf>-lysine.* Journal of Antibiotics, 1984. **37**(11): p. 1449-1455.
85. Fang, B., et al., *Antimicrobial surfaces containing cationic nanoparticles: HOW immobilized, clustered, and protruding cationic charge presentation affects killing activity and kinetics.* Colloids and Surfaces B: Biointerfaces, 2015. **125**: p. 255-263.
86. Zhou, C., et al., *A photopolymerized antimicrobial hydrogel coating derived from epsilon-poly-l-lysine.* Biomaterials, 2011. **32**(11): p. 2704-2712.
87. Ouyang, Y., et al., *Poly-l-lysine-modified reduced graphene oxide stabilizes the copper nanoparticles with higher water-solubility and long-term additively antibacterial activity.* Colloids and Surfaces B: Biointerfaces, 2013. **107**: p. 107-114.
88. Shan, C., et al., *Water-soluble graphene covalently functionalized by biocompatible poly-L-lysine.* Langmuir, 2009. **25**(20): p. 12030-12033.
89. Some, S., et al., *Dual functions of highly potent graphene derivative-poly-l-lysine composites to inhibit bacteria and support human cells.* ACS Nano, 2012. **6**(8): p. 7151-7161.
90. Wang, J., et al., *Synthesis of a hydrophilic poly-l-lysine/graphene hybrid through multiple non-covalent interactions for biosensors.* Journal of Materials Chemistry B, 2013. **1**(10): p. 1406-1413.
91. Hegab, H.M., et al., *The controversial antibacterial activity of graphene-based materials.* Carbon, 2016. **105**: p. 362-376.
92. Zeng, X., et al., *Graphene-based antimicrobial nanomaterials: rational design and applications for water disinfection and microbial control.* Environmental Science: Nano, 2017. **4**(12): p. 2248-2266.
93. Wang, X., et al., *A facile one-pot method to two kinds of graphene oxide-based hydrogels with broad-spectrum antimicrobial properties.* Chemical Engineering Journal, 2015. **260**: p. 331-337.
94. Asadishad, B., et al., *Transport, motility, biofilm forming potential andsurvival of Bacillus subtilis exposed to cold temperature and freeze-thaw.* Water Research, 2014. **58**: p. 239-247.
95. Ding, Z., et al., *Filtration and transport of heavy metals in graphene oxide enabled sand columns.* Chemical Engineering Journal, 2014. **257**: p. 248-252.
96. Ngwenya, B.T., P. Curry, and L. Kapetas, *Transport and viability of Escherichia coli cells in clean and iron oxide coated sand following coating with silver nanoparticles.* Journal of Contaminant Hydrology, 2015. **179**: p. 35-46.
97. Yousefi, N., et al., *Simultaneous in situ reduction, self-alignment and covalent bonding in graphene oxide/epoxy composites.* Carbon, 2013. **59**: p. 406-417.
98. Zheng, Q., et al., *Transparent conductive films consisting of ultralarge graphene sheets produced by Langmuir-Blodgett assembly.* ACS Nano, 2011. **5**(7): p. 6039-6051.

99. Hall, B.G., et al., *Growth rates made easy.* Molecular Biology and Evolution, 2014. **31**(1): p. 232-238.
100. Hurst, A., *Biosynthesis of the antibiotic nisin by whole Streptococcus lactus organisms.* Journal of general microbiology, 1966. **44**(2): p. 209-220.
101. Miles, A.A., S.S. Misra, and J.O. Irwin, *The estimation of the bactericidal power of the blood.* Journal of Hygiene, 1938. **38**(6): p. 732-749.
102. Bai, Y., et al., *Influence of graphene oxide and reduced graphene oxide on the activity and conformation of lysozyme.* Colloids and Surfaces B: Biointerfaces, 2017. **154**: p. 96-103.
103. Liu, Y., et al., *Physico- and bio-activities of nanoscale regenerated cellulose nonwoven immobilized with lysozyme.* Materials Science and Engineering C, 2018. **91**: p. 389-394.
104. Jahandideh, H., et al., *The Significance of Graphene Oxide-Polyacrylamide Interactions on the Stability and Microstructure of Oil-in-Water Emulsions.* Langmuir, 2018.
105. Kumar, A., B. Behera, and S.S. Ray, *Microwave-assisted surface-initiated redox polymerization of acrylamide with functionalized graphene oxide for aqueous lubricant additive.* RSC Advances, 2015. **5**(49): p. 39474-39481.
106. Ellison Iii, R.T. and T.J. Giehl, *Killing of gram-negative bacteria by lactoferrin and lysozyme.* Journal of Clinical Investigation, 1991. **88**(4): p. 1080-1091.
107. Masschalck, B., et al., *Inactivation of gram-negative bacteria by lysozyme, denatured lysozyme, and lysozyme-derived peptides under high hydrostatic pressure.* Applied and Environmental Microbiology, 2001. **67**(1): p. 339-344.
108. Khan, A., et al., *Optimization of the antimicrobial activity of nisin, Na-EDTA and pH against gram-negative and gram-positive bacteria.* LWT - Food Science and Technology, 2015. **61**(1): p. 124-129.
109. Theophel, K., et al., *The importance of growth kinetic analysis in determining bacterial susceptibility against antibiotics and silver nanoparticles.* Frontiers in Microbiology, 2014. **5**(NOV).
110. Lin, N., et al., *Nanodarts, nanoblades, and nanospikes: Mechano-bactericidal nanostructures and where to find them.* Advances in Colloid and Interface Science, 2018. **252**: p. 55-68.
111. Stevik, T.K., et al., *Retention and removal of pathogenic bacteria in wastewater percolating through porous media: A review.* Water Research, 2004. **38**(6): p. 1355-1367.

Appendix 1: Immobilization of Antimicrobial Agents by Electrostatic Interactions

In addition to studying the functionalization of GO surfaces by covalent methods, functionalization by electrostatic interactions was also investigated in early stages of the project. Although only lysozyme (LYS) was investigated in this context all of the chosen antimicrobial agents have a cationic character and were suitable for functionalization of the anionic graphene oxide structure. Functionalization was confirmed by evaluation of the surface chemistry by XPS analysis. The atomic percent of nitrogen was observed to increase in the GO/LYS sample functionalized by electrostatic interactions.

Table 8. XPS atomic composition results for GO/LYS nanocomposites prepared by physical interactions (electrostatic) and covalent methods (EDC/NHS coupling)

Condition	*C1s*	*O 1s*	*N 1s*
LYS	38.2 ± 8.6%	46.6 ± 11.5%	15.2 ± 3.9%
GO	53.3 ± 0.6%	46.7 ± 0.6%	n.d.*
GO/LYS (Physical)	65.3	30.4	2.6
GO/LYS (Covalent)	63.9	30.1	5.5

n.d. signifies "none detected"

The increase in nitrogen content was low, suggesting that functionalization by electrostatic methods was less effective than by covalent bond formation. Furthermore, disassociation of the antimicrobial agent from the GO surface is possible and therefore the longevity of the functionalized material is reduced.

Appendix 2: Evaluation of Degree of Functionalization by Spectroscopic Methods

Evaluation of immobilization degree of GO/LYS was performed by measuring the absorbance of the sample by UV-Vis spectroscopy with a wavelength of 280 nm. The absorbance spectra of lysozyme and graphene oxide are shown in (Figure 13). A calibration curve was generated to correlate the concentration of lysozyme solution to absorbance values at 280 nm as shown in (Figure 14).

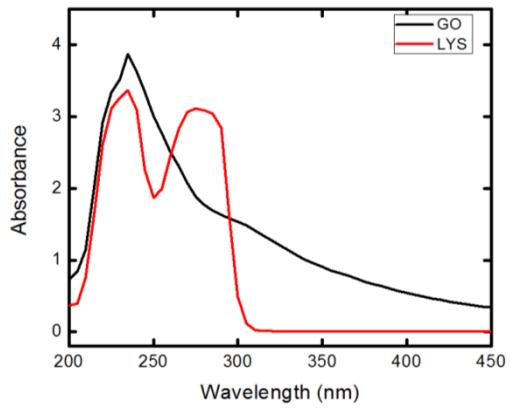

Figure 13. UV-vis absorbance spectra of GO and LYS.

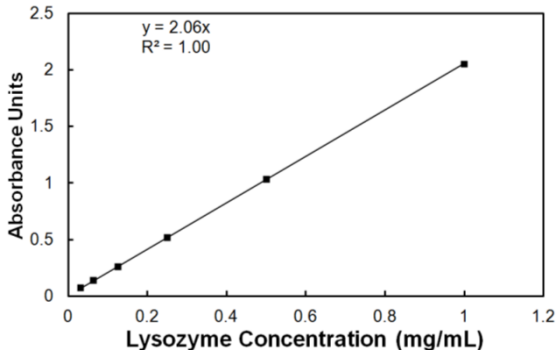

Figure 14. Calibration curve correlating lysozyme concentration and absorbance measured at a wavelength of 280 nm.

Absorbance measurements were performed before and after functionalization. Two control samples of lysozyme were also prepared, agitated and centrifuged, to ensure that decreased concentration measurements could be attributed to immobilization on graphene oxide and were not simply due to lysozyme settling.The degree of immobilization was calculated according to Equation 1.

***Equation* 1)** $$Percent\ immobilized\ \left(\frac{mg}{mg}\right) = 100\%\ x\ \frac{final\ concentration * 1mL - initial\ concentration * 1mL}{initial\ concentration * 1mL}$$

No significant decrease in lysozyme concentration was observed in the control samples and the immobilization degree of the control was $\pm 5\%$. The immobilization degree of lysozyme on graphene oxide by electrostatic interactions was on the order of 50-60%. However, the results varied widely between samples. Due to the overlap of the LYS and GO absorbance spectra and inefficiency of separation by centrifugation, this method for determining the functionalization degree was not suitable.

Appendix 3. XPS deconvoluted C1s and N1s peaks

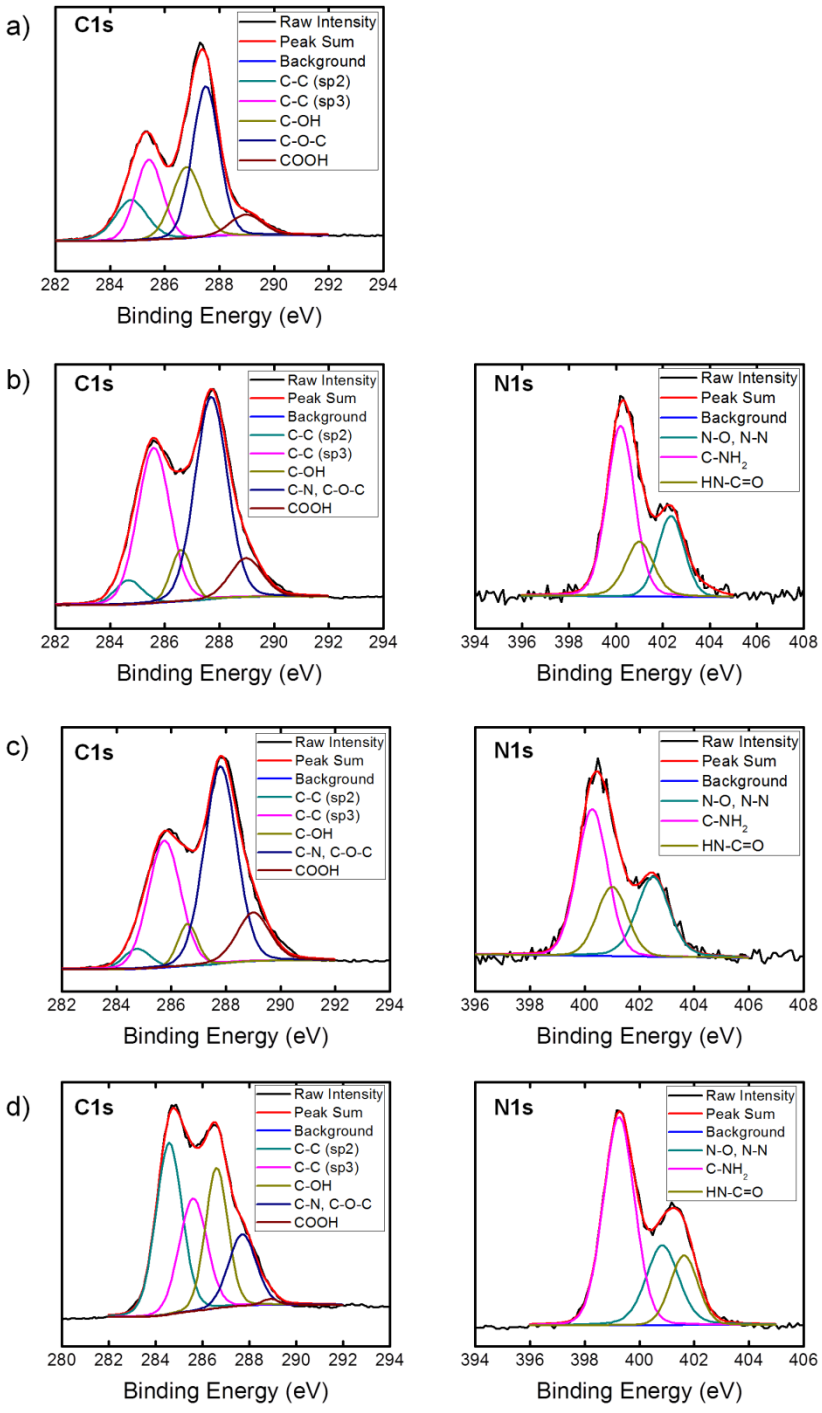

Figure 15. Deconvoluted XPS spectra of C1s and N1s peaks of a) GO, b) GO/NIS, c) GO/LYS, d) GO/PLL

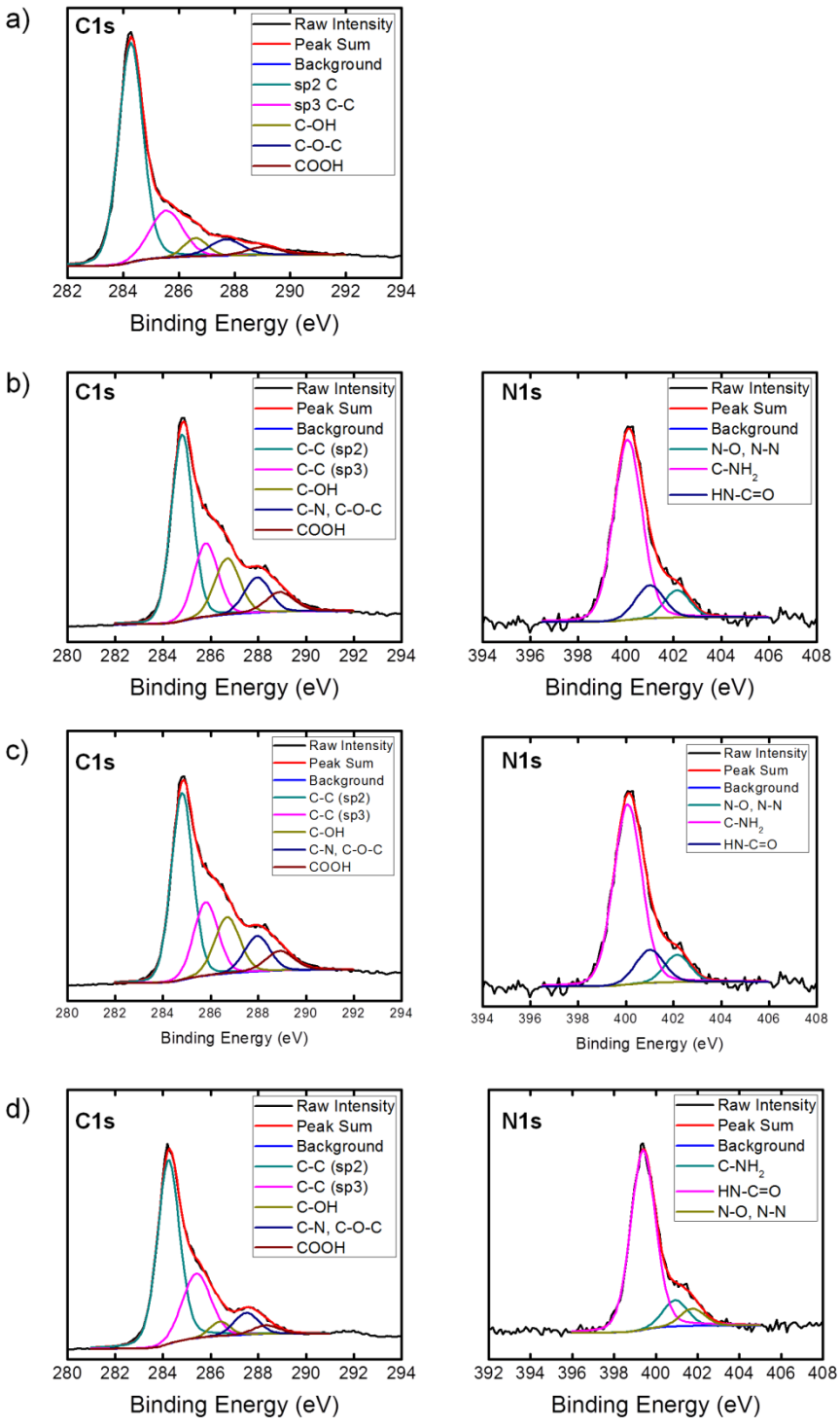

Figure 16. Deconvoluted XPS spectra of C1s and N1s peaks of a) sp-rGO b) sp-rGO/NIS c) sp-rGO/LYS d) sp-rGO/PLL

Appendix 4. FTIR spectra of functionalized nanoparticles

FTIR spectra were obtained and used to corroborate XPS evidence in order to confirm functionalization. The hydroxyl peak in the range of 300 cm-1 of the GO sample was significant compared to that of the sp-rGO due to the highly oxidized state. An additive effect of the spectra can be observed in the GO/NIS samples similar to that observed in the sp-rGO/NIS sample. However, in the GO/LYS the same peak broadening does not occur and distinct peaks may be identified. Namely those of the Amide I and Amide II features found around 1650 cm-1 and 1540 cm-1 respectively. It is likely that a conformational change induced by the freeze drying sample preparation of the sponge samples may have caused the peak broadening in the sp-rGO/LYS sample, which did not occur in the air dried thin film sample of GO/LYS.

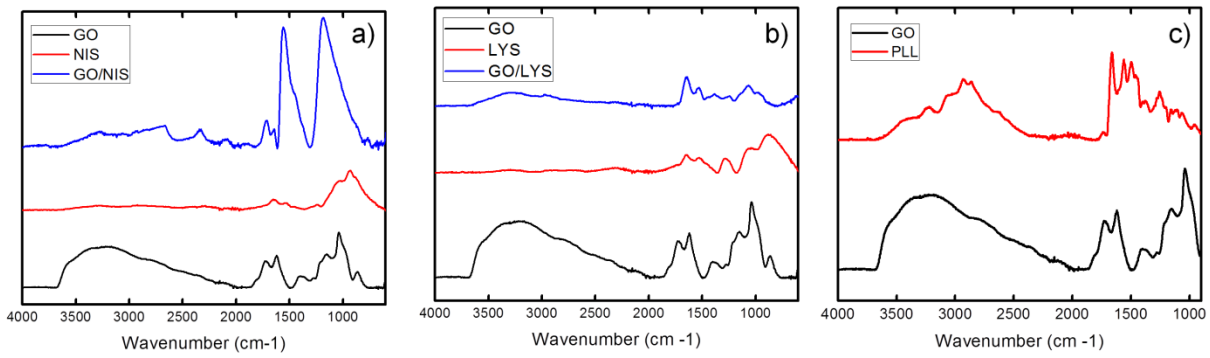

Figure 17. FTIR spectra of thin film samples of GO, antimicrobial agents and functionalized nanoparticles.

Appendix 5: Reaction ratio and its effect on surface chemistry, zeta-potential, and antimicrobial properties

Two reaction ratios were investigated for the GO/NIS and GO/LYS materials. XPS analysis confirmed that an increase in GO:NIS or GO:LYS reaction ratio from (2:1) to (1:1) lead to a comparable increase in atomic nitrogen content as shown in the table below.

Material	C1s	O1s	N1s
GO	53.3 ± 0.6%	46.7 ± 0.6%	n.d.*
GO/NIS (2:1)	64.9 ± 0.7 %	29.0 ± 0.3%	6.1 ± 0.1%
GO/NIS (1:1)	63.5 ± 0.6%	24.2 ± 0.9%	12.3 ± 0.6%
GO/LYS (2:1)	64.1 ± 0.2 %	30.6 ± 0.5 %	5.3 ± 0.3%
GO/LYS (1:1)	60.3 ± 0.4%	29.0 ± 0.9%	10.7±0.5%

* n.d. signifies "none detected"

Various reaction ratios were tested with the GO/NIS material. Zeta-potential increased in all samples relative to the non-functionalized GO material. Furthermore, as the GO:NIS ratio was increased from 4:1 to 2:1 the zeta-potential increased suggesting that the larger quantity of cationic nisin is increasing the positive charge on the material. At the 1:1 ratio a further increase in zeta-potential was not observed.

Material	Zeta-Potential (ζ)
GO	-48 ± 3
GO/NIS (4:1)	-37 ± 2
GO/NIS (2:1)	-26 ± 1
GO/NIS (1:1)	-36 ± 1

A single replicate of a growth inhibition assay with *B. subtilis* was performed and the growth behaviour in the 4:1 and 2:1 ratios differed, where the higher nisin content resulted in inhibition of growth. However, in both experiments, the final OD values were very high and further study is needed to confirm this effect.

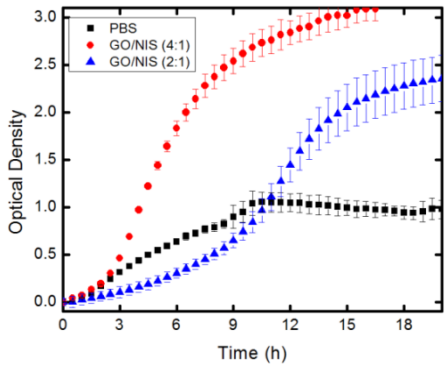

Figure 18. Growth profile of *B. subtilis* exposed to GO/NIS prepared at different reaction ratios.

Appendix 6: Concentration dependent growth behavior of *B. Subtilis* and *E. coli* exposed to antimicrobial agents and functionalized nanoparticles

LYS showed antimicrobial activity against *B. subtilis* with the MIC found to be on the order of 0.100 mg/mL. Evidence of growth inhibition was observed even at lower concentrations as evidenced by the prolonged lag phase. By contrast, LYS did not inhibit bacterial growth of *E. coli* at the concentrations tested. While a slight, statistically significant decrease in growth can be observed, the final optical density was reduced only by roughly 10%. Initial growth inhibition tests with NIS were carried out in dilute HCl solution (0.01 M) as recommended in the product data sheet by the supplier. However, when the growth inhibition experiment was repeated in phosphate buffered saline (PBS), the MIC was only achieved at 16 mg/mL. Such a result was obtained in replicate. This suggests that efficacy of NIS is increased in an acidic environment, and highlights the importance of the buffer choice in the system. PLL had bacteriostatic antimicrobial activity against both *B. subtilis* and *E. coli.* At sub-MIC concentrations anti-microbial activity was still observed as evidenced by a change in growth rate and extended lag phase.

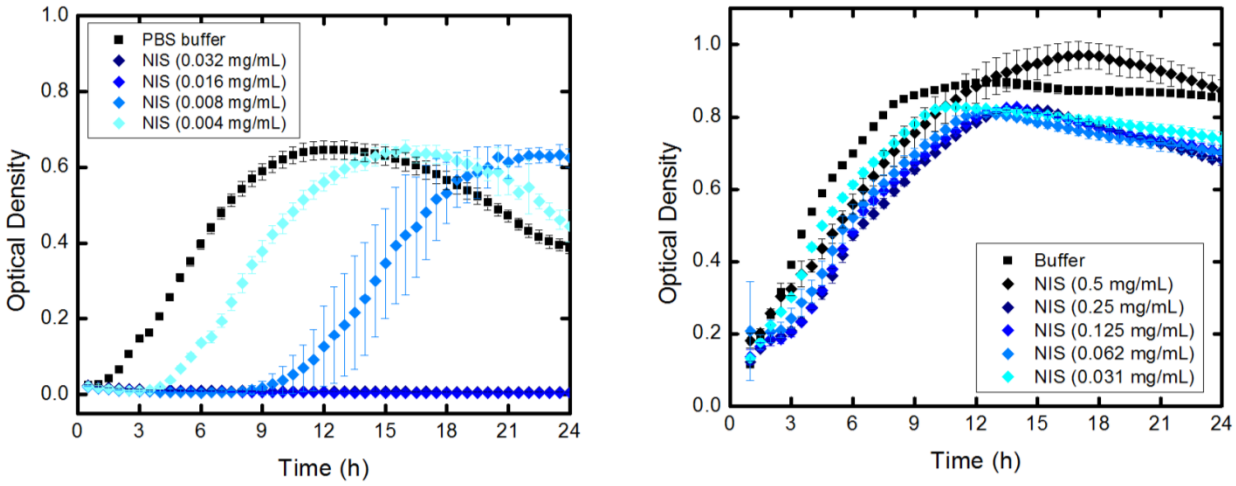

Figure 19. Minimum inhibitory concentration growth profiles for *B. subtilis* (left) and *E. coli* (right) exposed to NIS.

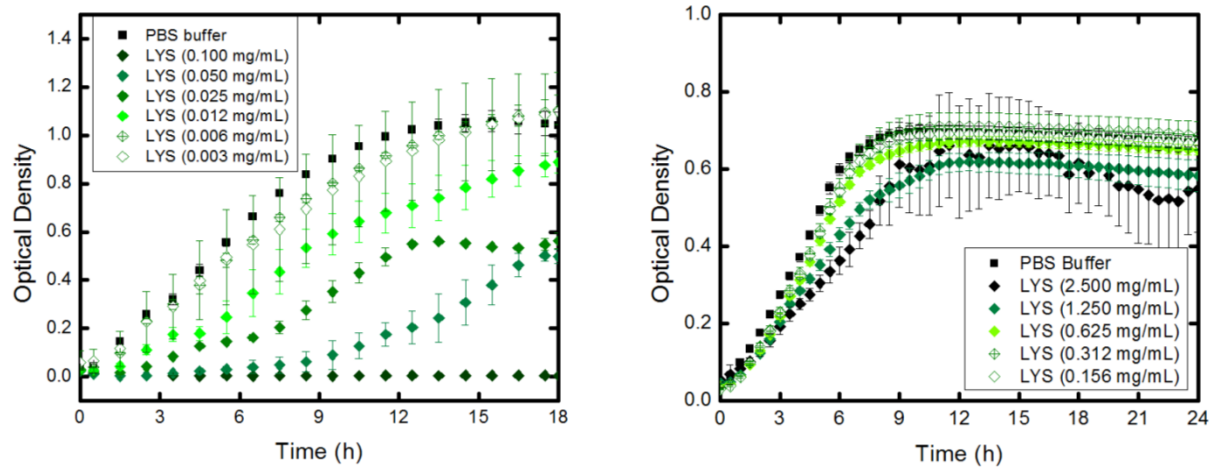

Figure 20. Minimum inhibitory concentration growth profiles for *B. subtilis* (left) and *E. coli* (right) exposed to LYS.

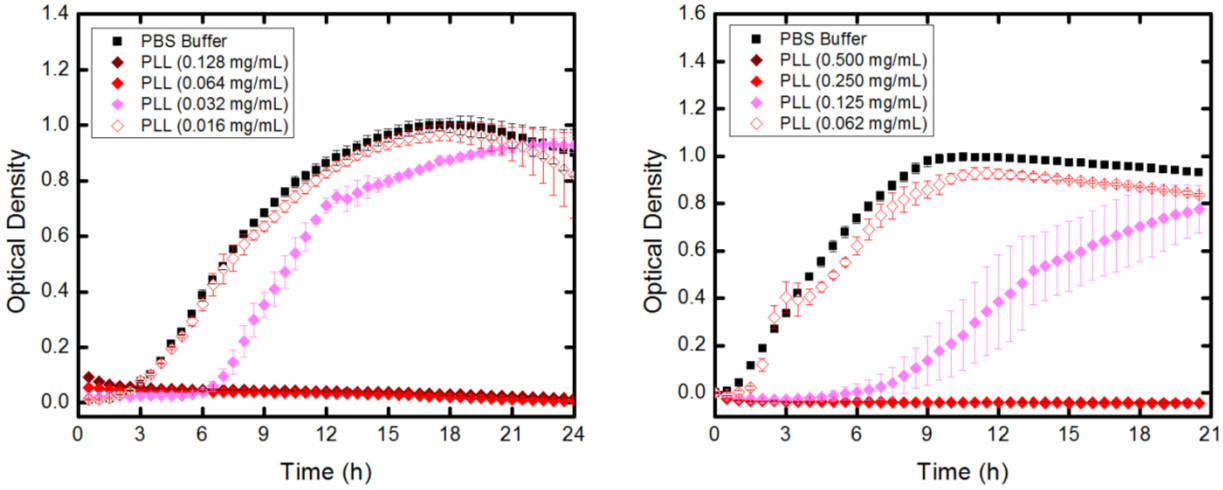

Figure 21. Minimum inhibitory concentration growth profiles for *B. subtilis* (left) and *E. coli* (right) exposed to PLL.

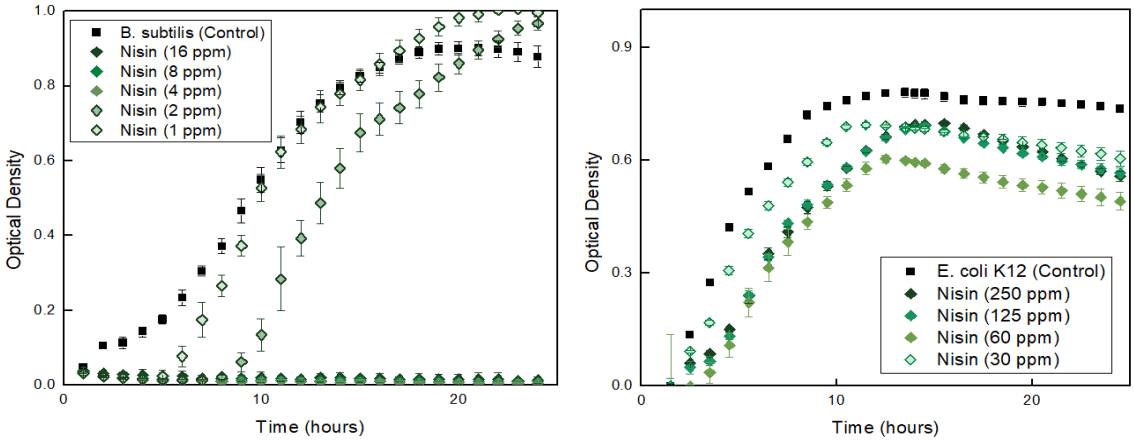

Figure 22. Representative growth profiles for a) *B. subtilis* with Nisin (0.01M HCl) b) *E. coli* with Nisin (0.01M HCl)

Previously, the behavior of functionalized nanoparticles (GO/Nis and GO/Lys) as well as graphene oxide control (GO) were not evaluated in nutrient broth overnight by UV-vis measurements. An increase in optical density was observed in the nanoparticle conditions without bacteria. The increase in optical density is more pronounced in higher concentrations as shown in the graphs below. This effect suggests that the increase in optical density can be correlated to an aggregation effect rather than contamination and bacterial growth. The aggregation effects are rarely discussed in the literature, and these results highlight that optical density measurements, while convenient, may not be suitable for evaluation of antimicrobial activity of suspended materials. A concentration of 0.25 mg/mL was chosen for other antimicrobial assays as this was the highest nanoparticle concentration possible for which significant suspension instability and aggregation did not occur.

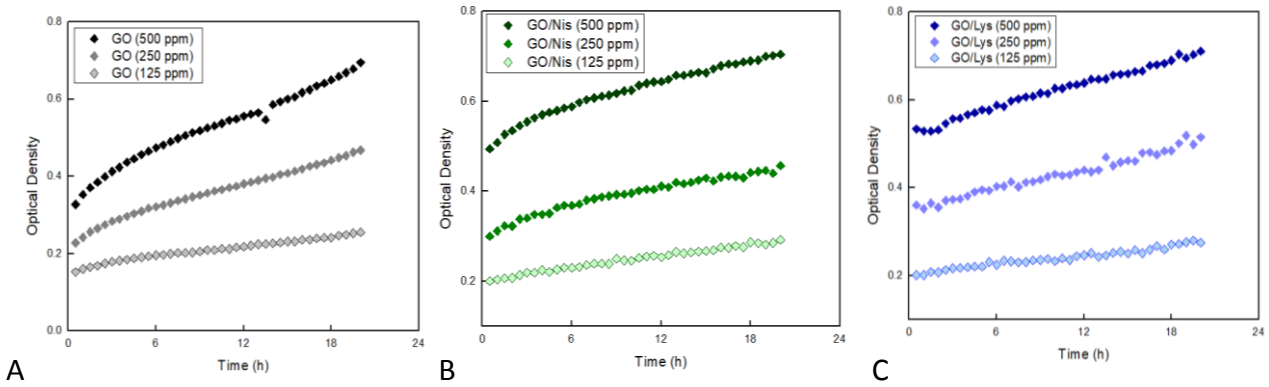

Figure 23. Optical density measurements of negative control conditions showing apparent aggregation behavior in a) GO, b) GO/NIS and c) GO/LYS condtions.

The effect of functionalized nanoparticle concentration was investigated against *B. subtilis*. Some concentration dependent behavior was observed, particularly in the GO/NIS and GO/LYS conditions although this effect was minimal.

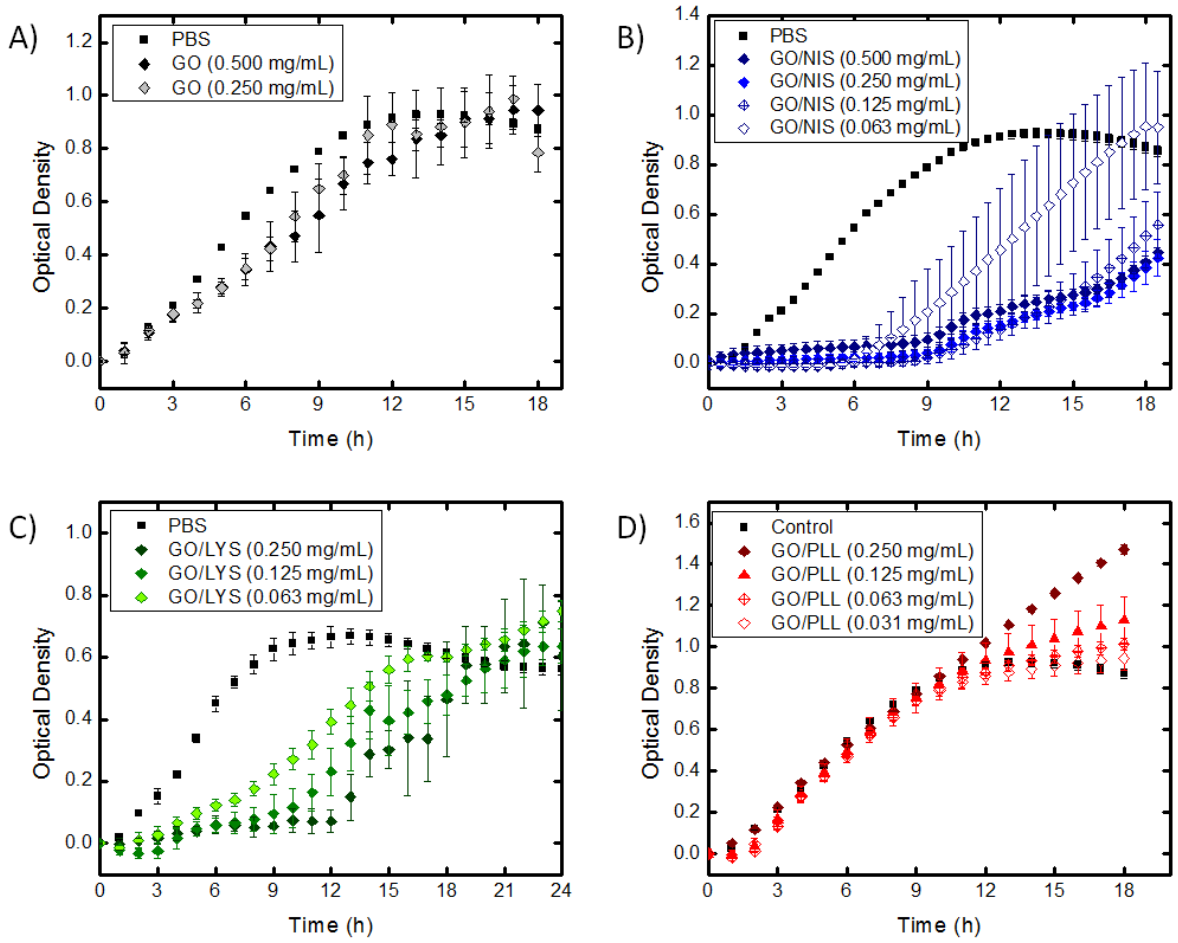

Figure 24. Concentration dependent growth behavior of *B. subtilis* exposed to A) GO, B) GO/NIS C) GO/LYS D) GO/PLL

Appendix 7: Inactivation of *B. Subtilis* by functionalized nanoparticles

While cell growth inhibition is an indicator of antimicrobial activity, alone cell growth inhibition assays do not confirm that cell death occurs upon exposure to the antimicrobial agent. In order to evaluate bactericidal behavior cell inactivation behavior or cell death rate was accessed. Cells were harvested in mid-exponential phase, washed and re-suspended in phosphate buffer (OD_{600}=1.0). Antimicrobial agents were prepared in various concentrations in phosphate buffer and added in a 1:1 ratio to the bacterial suspension. For the control condition, PBS buffer with no antimicrobial agent was added in a 1:1 ratio to the bacterial suspension. Samples were incubated at 35.5 degrees Celsius under agitation. Samples of 20µL were obtained at various time points throughout the total incubation time of 24 hours. Colony forming units (CFU) counts were obtained by drop plating onto LB agar plates.

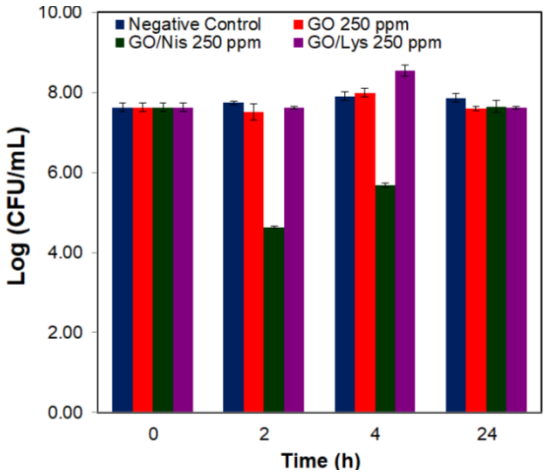

Figure 25. Inactivation of *B. subtilis* upon exposure to functionalized nanoparticles.

A decrease in culturability was observed in the GO/NIS condition after 2 and 4 hours. However, the culture appears to recover after 24 hours. It is possible that this is a result of inactivation of the antimicrobial material with time or due to the high number of cells in the inactivation assay which may have lead to aggregation effects or saturation of the nanomaterial. No statistically significant change was observed in the GO/LYS condition. In order to better understand the system, microscopy methods were undertaken and BacLight Live/Dead staining was performed after long term exposure (15 hours) in order to understand impact on viability and membrane integrity.

Appendix 8: Modified Disk Assay

In order to understand the antimicrobial activity of the functionalized sponge material a modified disk assay was attempted. Briefly, an overnight culture of *Bacillus subtilis* ATCC 6633 strain was prepared and 100 μL of culture was spread onto agar plates using a sterile cell spreader. To test the antimicrobial activity of the sp-rGO/LYS hydrogel slice, the sample was flattened by pressing to remove the porous structure, in order to improve contact with the agar plate. As a negative control a sp-rGO hydrogel slice with no antimicrobial agent, was similarly washed and flattened. Agar plates were subdivided into four quadrants and labeled as shown below**.** Negative control plates were also similarly subdivided, however no *B. subtilis* was added in this case. This negative control condition was used to evaluate if the hydrogel itself was contributing to any contamination.

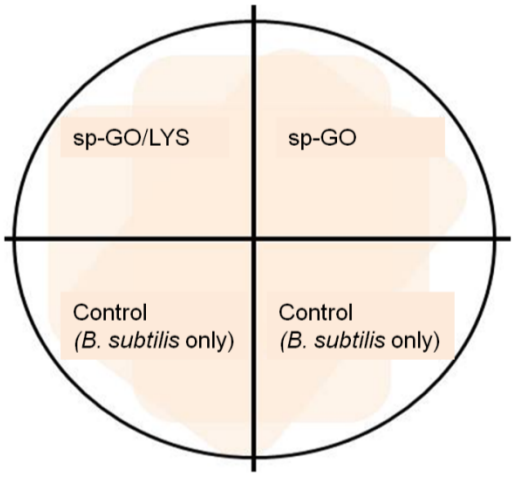

Figure 26. A schematic of experiment configuration for the modified disk assay.

No growth was observed in the region in contact with the hydrogel. This was the case for the control sp-rGO and functionalized sp-rGO/LYS. While result might be interpreted as potent antimicrobial activity, such a conclusion is unlikely. It was hypothesized that oxygen transfer limitations imposed by the hydrogel, absorption of moisture by the hydrophilic hydrogel surface, or bacteria adherence to the sponge may have prevented growth of bacteria on the agar plate. The results of this assay were assessed to be unreliable and microscopy techniques were selected to evaluate the antimicrobial properties of the functionalized hydrogel system.

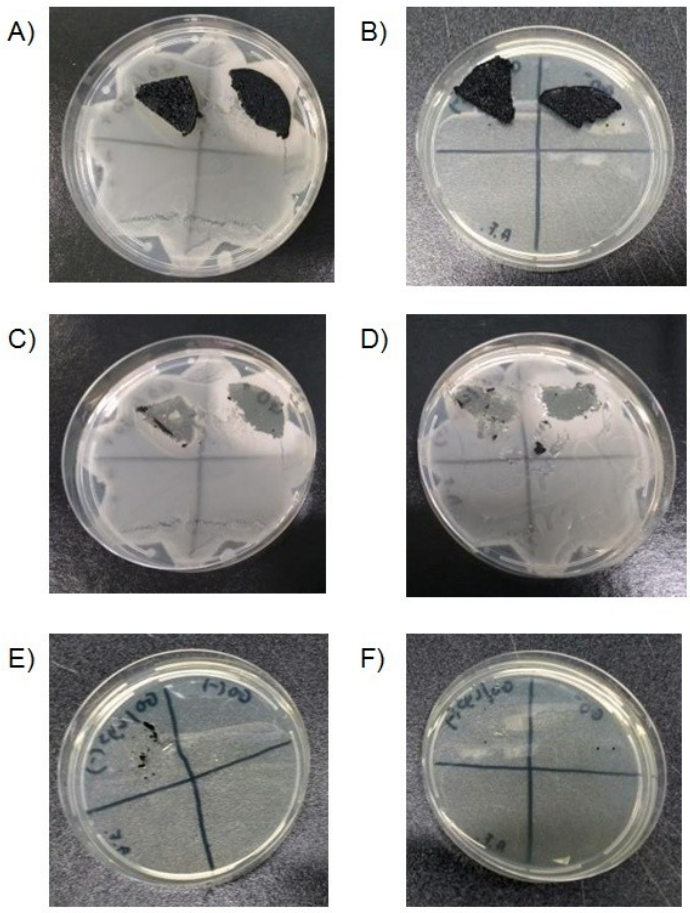

Figure 27. a) Experiment setup after overnight growth of bacterial lawn b) Experimental set up after overnight incubation of negative control condition c, d) Experimental samples with *B. subtilis* lawn. sp-rGO/LYS (top left quadrant), sp-rGO (top right quadrant), positive control (bottom right, left quadrants) e,f) Control samples with no bacteria. sp-rGO/LYS (top left quadrant), sp-rGO (top right quadrant), negative control (bottom right, left quadrants).

Appendix 9. Growth inhibition of *B. subtilis* by functionalized hydrogel

Tissue culture (companion) plates were used to evaluate the growth inhibition of *B. subtilis* in the presence of sp-rGO/LYS and sp-rGO/NIS. Companion plate sieves with a pore size of 8 micron were used to contain the sponge material. The pore size is large enough to permit bacteria to pass through, but remained small enough to enable simple removal of the sponge material. The reduction in bacteria growth by the functionalized sponges was determined by measuring the optical density and CFU count at 0 hours and 18 hours. The growth of *B. subtilis* was reduced by 50% in sp-rGO/NIS condition relative to the control condition in which *B. subtilis* was not exposed to sponge material. The growth of *B. subtilis* was unaffected by the presence of sp-rGO/LYS. It is possible that the effective concentration of lysozyme was not sufficient to inhibit growth as the MIC of lysozyme against *B. subtilis* was much higher than the MIC of nisin. However, sub MIC effects such as extended lag phase might still be observed at earlier time points, although these time points were not evaluated in this experiment. It is also possible that conformational changes to the lysozyme structure during functionalization may have reduced the efficacy.

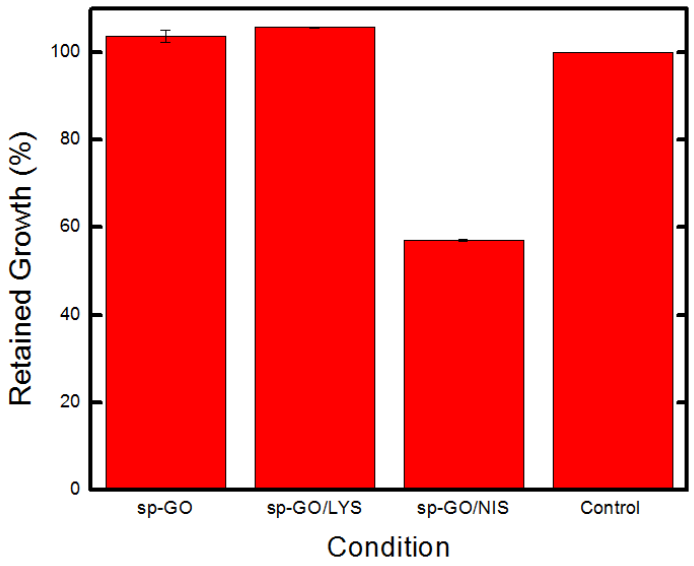

Figure 28. Retained growth (%) of *B. subtilis* exposed to functionalized sponges after 18 hours. Results are normalized to the control condition: *B. subtilis* grown in LB only.

Appendix 10. Additional Images of *B. subtilis* and *E. coli*

Additional microscopy images of the two model organisms are provided.

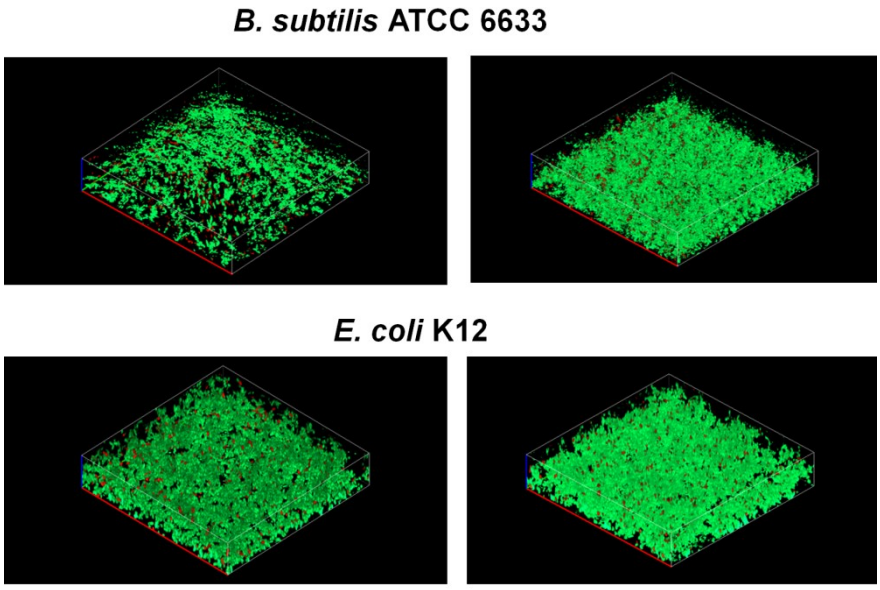

Figure 29. Control CLSM images of *B. subtilis* and *E. coli* (OD_{600}= 1) incubated with PBS buffer for 15 hours at 35.5 °C.

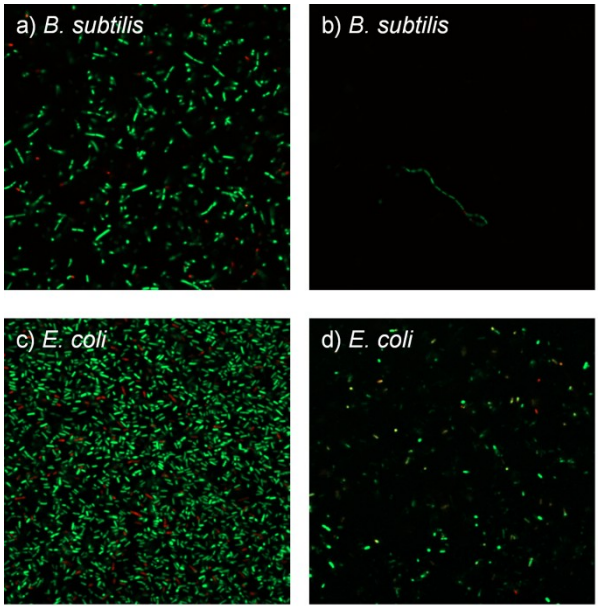

Figure 30. Fluorescence microscopy images showing chain-forming behavior in *B. subtilis*. No chain-forming behavior is observed in *E. coli*.

Appendix 11. Calibration curve of *B. subtilis* ATCC 6633

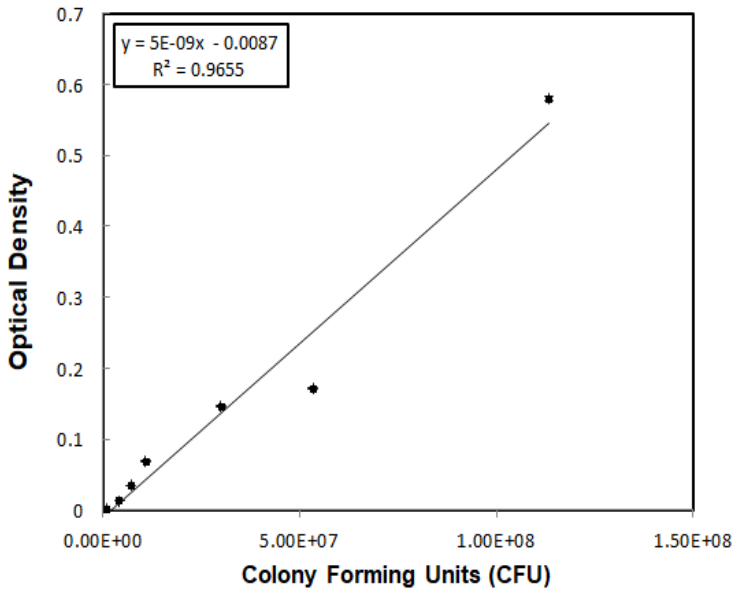

Figure 31. Calibration curve of *B. subtilis* ATCC 6633